Periodic "stick-slip" transition within a continuum model for entangled supramolecular polymers

Victor A. H. Boudara and Daniel J. Read*

School of Mathematics, University of Leeds, LS2 9JT Leeds, U.K.

(Dated: November 1, 2017)

Abstract

We investigate shear flow instabilities using a recently-derived constitutive law, designed for describing the rheology of entangled telechelic polymers. The continuum model displays shear banding, often accompanied by a strong elastic recoil in the transient response, which appears as an "apparent" wall slip. For certain parameters, the model also displays a novel "apparent" stick-slip behavior, giving rise to strong nonlinear oscillations in the stress response driven by a repeating cycle of elastic recoil followed by diffusive rehomogenization of the flow. We elucidate the detailed mechanism behind this oscillatory response, demonstrating that it arises from a competition between shear-induced breaking of sticky bonds, which leads to recoil and banding, and a diffusive rehomogenization of the flow. We discuss the relation between the apparent stick-slip in our continuum model with similar behavior in "true" wall slip.

---

* d.j.read@leeds.ac.uk

I. INTRODUCTION

The flow of viscoelastic liquids is often accompanied by interesting effects usually not seen in (simple) Newtonian liquids [1–7]. Non-Newtonian effects are frequently present during the extrusion of molten polymers at high stresses – one of the most common industrial shaping process. The surface or shape of the resulting material is altered by the presence of flow defects such as extrudate swelling, crystallization effects, sharkskin or melt flow instabilities, depending on the type of polymer as well as on the construction of the capillary device [4, 8–10]. In some constant rate experiments on capillaries [11, 12] or cone-plate geometry [13, 14], a periodic oscillation of the shear stress or pressure is observed and attributed to either a structural breakdown (chain disentanglement), or to a stick-slip transition at the walls or between macrodomains [14]. These instabilities can alter the flow and final properties of the material and therefore controlling these phenomena is of critical industrial importance in the processing of polymers.

We focus on the specific phenomenon of wall slip. A non-zero relative velocity at a solid-liquid interface is called "true slip". This must be carefully distinguished from "apparent slip" which is a phenomenon related to shear banding. For example, when we impose an external shear rate, higher than the complex-fluid characteristic time, the internal mesoscopic structure is reorganized and the shear rate may localize so that two (or more) bands experiencing different shear rates coexist. In the resulting "shear banded" state, a narrow shear band close to a wall can appear as an apparent wall slip, and in practice it can be difficult to distinguish true wall slip from apparent slip. This illustrates a more general point, that different types of explanation are advanced for many of the problematic processing phenomena such as shark skin, wall slip, gross melt fracture. Some phenomena are elastic or bulk in origin, coming from an instability in the bulk of the material. Gross melt fracture would be an example, as is "apparent" wall slip. Such phenomena can be investigated by examining the bulk rheological behaviour of the material in question. Other instabilities are related to the local molecular physics and chemistry near the wall or free surface, and so require investigation of that local environment. "True" wall slip would be an example of this. For more details, see Refs. [15, 16] for reviews on wall slip and instabilities, and Ref. [17] for a handbook on polymer fracture.

Shear banding is ubiquitous in complex fluids and has been reported in systems such as
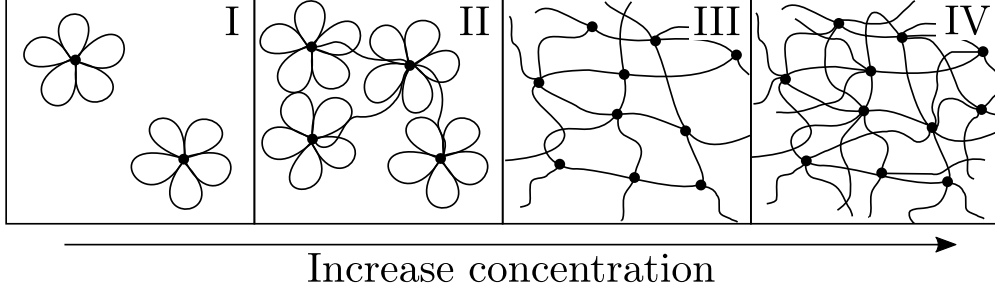
Increase concentration

FIG. 1. Sketch of the typical network structure of linear telechelic chains. At low concentration, telechelic chains assemble into flowerlike micelles, i.e. mainly loops are formed (I). Upon increasing concentration, some bridges between micelles appear (II), until the point where bridges are the most energetically-favorable configurations, and typically there is overlap between chains (III). Finally, at "high" concentration, the chains overlap enough to become entangled (IV).

wormlike micellar surfactant solutions, polymer solutions and melts, star polymers, emulsions, suspensions, microgels, biological gels, and foams [18]. Since the first theoretical models for wormlike micelles [19–22], numerous techniques and experiments were developed to understand the shear banding phenomenon; see [23–26] for reviews of experiments (mainly on wormlike micelles) and theoretical considerations. Experimental understanding of the flow and instabilities in complex fluids generally rely on rotational rheometers [27], e.g. Taylor-Couette, cone-plate, or parallel plate geometries. Polymeric systems with reversible junctions, such as entanglements or associative stickers, are also known to undergo flow instabilities, e.g. spurt [28], shear banding [18, 24, 29–32] or melt fracture [33–35]. In concentrated solutions of telechelic polymers, i.e. linear chains with stickers at both extremities that enable the formation of transient network, experiments [33, 36, 37] and MD simulations [38] showed that flow instabilities can occur.

In this paper, we will examine shear banding instabilities present in a particular constitutive model, the preaveraged constitutive model for entangled telechelic star polymers (PETS) [39]. We demonstrate that this model can produce both apparent wall slip, and an apparent stick-slip oscillation. The PETS model was developed from a molecular picture of entangled star polymers with sticky groups at the ends of the star arms. It was argued that the star architecture provided the simplest system for consideration of the combined effects of entanglements and sticker dynamics in a non-linear model (because a star arm is a two state system, in which the sticker is either attached, or detached). However, the

3

model may also be applicable in many more general situations where sticky interactions and entanglements are both present, such as telechelic linear chains, as we now discuss. Above a critical concentration, telechelic polymers self-assemble into overlapping flowerlike micelles whose local structure resembles star polymers. Indeed, in the limit of very sticky systems, linear entangled telechelic polymers have both ends attached most of the time and, upon (rare) detachment of a sticker, the linear polymer is in a configuration akin to star polymers with one anchored end (branch point) and one free end. Fig. 1 sketches the effect of increasing concentration of linear telechelic chains on the network structure. At low concentration, telechelic chains assemble into flowerlike micelles, i.e. mainly loops are formed (I). Upon increasing concentration, some bridges between micelles appear (II), until the point where bridges are the most energetically-favorable configurations, and typically there is overlap between chains (III). Finally, at "high" concentration, the chains overlap enough to become entangled (IV). The onset of entanglements would occur whether or not the chains also have telechelic end groups, provided the chains are sufficiently concentrated. Note that Refs. [40, 41] are typical models for the unentangled regime (III), and that these models have a similar "two state" (attached and detached) structure to the PETS model. In this work, we focus on regime (IV), where the PETS model [39] typically applies if the stickers have a long lifetime and most of the stickers are associated at equilibrium. These conditions translate in the notation of this work into $\tau_{as} \gg \tau_s$ and $\phi_{as} \gg 1$ (see Section II A for definitions).

In summary: we investigate shear banding using the preaveraged constitutive model for entangled telechelic star polymers (PETS) [39] and compare with experimental findings on concentrated solution of linear telechelic chains. We show that a molecular constitutive model for entangled telechelic polymers predicts (i) steady state shear banding and (ii) periodic oscillatory stress response. These oscillations are generated by an "apparent slip" i.e. a narrow shear band usually close to the wall, giving the impression of a "stick-slip" behavior (though our simulations use non-slip boundary conditions). In contrast with phenomenological models of, e.g., Refs. [42, 43], our molecular model reveals a novel mechanism for a stick-slip transition, arising from interaction between the structural relaxation within the material, and diffusion of the constituent species across a narrow band. In what follows, we present our model, the mechanism of this apparent stick-slip process, and discuss how this may relate to the non-trivial physical phenomena occurring in experiments. We also discuss

whether a similar diffusive mechanism may be at work for oscillatory behavior in true wall slip.

II. PREAVERAGED CONSTITUTIVE MODEL FOR ENTANGLED TELECHELIC STAR POLYMERS

A. Origins of the PETS model
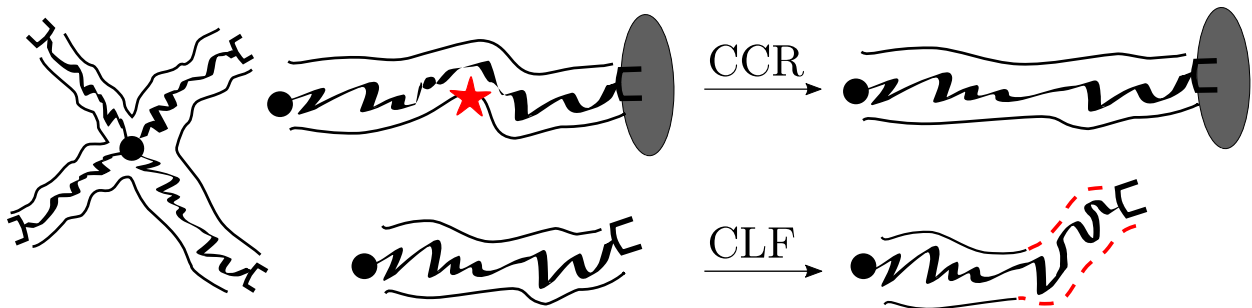
FIG. 2. Each star-arm has a sticky group "⊏" on one end, and is fixed to the branch point "•" on the other end. Top: the sticker is attached (to the gray area), CCR event (red star) contributes to stress relaxation. Bottom: the sticker is detached, CLF relaxes stress by renewing the tube (dotted line)–in addition to CCR.

As a toy (i.e. single mode) model combining entanglements and stickers, we previously developed a *stochastic* model for entangled telechelic star polymers [39]. This considers an ensemble of star arms where each arm has its own history of sticker attachment and detachment. Additionally, each star arm is entangled, and we used the Rolie-Poly model (RP) [44] to account for the entanglement effects. The advantage of the RP model [44] over, e.g., the Johnson-Segalman model (a widely used phenomenological constitutive model [45, 46]) is that it is derived from a full molecular model based on tube dynamics, and it includes chain stretch, contour length fluctuation, and thermal and convective constraint release (CCR) [47]. When detached, all relaxation mechanisms included in the RP model are possible: orientation relaxation, stretch relaxation, contour length fluctuations (CLF), and convective constraint release (CCR). When attached, the arm is pinned between the star branch point and the sticker, thus it cannot relax its orientation or stretch, however, CCR is still possible, see Fig. 2. In reality, for an attached arm with Z entanglements, there

should be a spectrum of Z Rouse modes associated with CCR; the fact that the ends of the arm are pinned means that the longest mode cannot relax stress by CCR, but the remaining $(Z-1)$ internal modes are free to relax stress. In the single-mode Rolie-Poly approximation to this situation, we choose to allow CCR to relax the stress on attached arms.

The dynamics of attachment/detachment of the sticker is essentially controlled by τ_{as} and ϕ_{as}, the average time a sticker stays associated at equilibrium, and the fraction of associated sticker at equilibrium, respectively. Note that a third parameter, τ_{free}, being the typical time a sticker stays free, is constrained by the above two by

$$\tau_{\mathrm{free}} = \tau_{\mathrm{as}}(1 - \phi_{\mathrm{as}})/\phi_{\mathrm{as}}. \tag{1}$$

All the "sticky features" of the material are contained in τ_{as} and ϕ_{as}. Temperature or chemical modification of the solvent may affect the strength of the stickers. For example, an increase of temperature deactivates hydrogen bonds; counter-ions inactivates metal-ligands stickers [48–50]. These might also affect the rate at which supramolecular bonds are formed and broken. Therefore, a so-called "sticky" system (ϕ_{as} close to 1) can have either a fast or slow rate of bond formation and breaking. All these parameters are contained in ϕ_{as} and τ_{as}.

The detachment is considered as an activated process. Attached stickers are residing within an energy well, so that they must overcome an energy barrier in order to detach [51]. The rate of detachment, r_{det}, is a function of the arm stretch: it increases as the arm is stretched, i.e. when the arm pulls on an attached sticker, it lowers the energy barrier that the sticker must overcome in order to detach.

In summary the stochastic model considers an ensemble of N_{c} arms, each arm i has his sticker either attached or detached. When the sticker is attached, we use [39]

$$r_{\mathrm{det}}(\lambda_i) = \tau_{\mathrm{as}}^{-1} \left(\frac{1 - \lambda_i^2 \lambda_{\mathrm{max}}^{-2}}{1 - \lambda_{\mathrm{max}}^{-2} \left(\lambda_i - \frac{r}{Za_0} \right)^2} \right)^{-\frac{3}{2} Z \lambda_{\mathrm{max}}^2}, \tag{2}$$

$$\frac{\mathrm{d}\boldsymbol{A_i}}{\mathrm{d}t} = \boldsymbol{\kappa} \cdot \boldsymbol{A_i} + \boldsymbol{A_i} \cdot \boldsymbol{\kappa}^{\mathrm{T}} - 2\beta\nu\lambda_i^{2\delta}(\boldsymbol{A_i} - \boldsymbol{I}). \tag{3}$$

6

When the sticker is detached, we use:

$$r_{\text{att}} = \tau_{\text{free}}^{-1}, \tag{4}$$

$$\frac{\mathrm{d}\boldsymbol{A_i}}{\mathrm{d}t} = \boldsymbol{\kappa} \cdot \boldsymbol{A_i} + \boldsymbol{A_i} \cdot \boldsymbol{\kappa}^{\mathrm{T}} - 2\beta\nu\lambda_i^{2\delta}(\boldsymbol{A_i} - \boldsymbol{I}) \tag{5}$$

$$-\frac{1}{\tau_{\mathrm{d}}}(\boldsymbol{A_i} - \boldsymbol{I}) - \frac{2(1 - \lambda_i^{-1})}{\tau_{\mathrm{s}}}\,\mathrm{f_E}(\lambda_i)\boldsymbol{A_i},$$

where $\boldsymbol{A_i}$ is the conformation tensor of the arm i, $\boldsymbol{\kappa}$ is the velocity gradient tensor, τ_{d} and τ_{s} are the orientation and stretch relaxation times of the (unattached) arms, $\mathrm{f_E}$ is a finite extensibility function, (β, δ) are the CCR parameters, ν is the CCR rate averaged over the ensemble of arms, and $\lambda_i = (\mathrm{tr}\,\boldsymbol{A_i}/3)^{1/2}$ is the stretch ratio of the arm i. Eqs. (2) and (4) are the rates of detachment and attachment of the stickers. Note that r_{det} diverges when the stretch (of an attached chain) approaches the maximal stretch ratio λ_{max}: increased forces in the polymer chain promotes detachment of the sticker. Eqs. (3) and (5) are the evolution equations that the conformation tensor, $\boldsymbol{A_i}$, of the chain i, follows when its sticker is associated or free, respectively. The total stress, $\boldsymbol{\sigma}$, in units of G, is then

$$\boldsymbol{\sigma} = \frac{1}{N_{\mathrm{c}}} \sum_{i=1}^{N_{\mathrm{c}}} \mathrm{f_E}(\lambda_i)\boldsymbol{A_i}. \tag{6}$$

B. Towards flow computation

The stochastic model, just described, was in good qualitative agreement with linear rheology data of entangled telechelic stars [52]. In nonlinear flows, the stochastic model exhibits a non-monotonic flow curve for (reasonable) parameter values typical of supramolecular systems in the absence of supramolecular interactions [39, 52], and for RP parameters $(\beta, \delta) = (1, -0.5)$, known for producing a *monotonic* flow curve in the non-telechelic Rolie-Poly model [44]. However, the stochastic model is not very efficient for numerical computation in complex flows such as shear banding calculations because of the cost of solving stochastic equations for many arms. Given this, we developed the PETS model – a preaveraged version of the stochastic model briefly presented above in Section II A – which is far less computationally costly and retains most of the features of the stochastic model. The PETS model predictions closely match the stochastic model, and it is suitable for flow computation.

The stress tensor, $\boldsymbol{\sigma}$, in the PETS model, is written as a linear combination of stress from arms with attached and detached stickers

$$\boldsymbol{\sigma} = f\boldsymbol{Q}_\mathrm{A} + (1-f)\boldsymbol{Q}_\mathrm{D}. \tag{7}$$

The dynamical variables are: f, the instantaneous fraction of attached stickers, and $\boldsymbol{Q}_\mathrm{A}$ and $\boldsymbol{Q}_\mathrm{D}$, the averaged stress (including maximum stretch) from Attached and Detached chains, respectively. The full dynamical equations of the PETS model are derived in Ref. [39] and reproduced in Table I, but may be written schematically as:

$$\frac{\mathrm{d}f}{\mathrm{d}t} = (1-f)\,r_\mathrm{att} - f\,r_\mathrm{det}, \tag{8}$$

$$\frac{\mathrm{d}\boldsymbol{Q}_\mathrm{A}}{\mathrm{d}t} = \left.\frac{\mathrm{d}\boldsymbol{Q}_\mathrm{A}}{\mathrm{d}t}\right|_{\mathrm{flow,CCR}} + r_\mathrm{att}\frac{1-f}{f}\left(\boldsymbol{Q}_\mathrm{D} - \boldsymbol{Q}_\mathrm{A}\right), \tag{9}$$

$$\frac{\mathrm{d}\boldsymbol{Q}_\mathrm{D}}{\mathrm{d}t} = \left.\frac{\mathrm{d}\boldsymbol{Q}_\mathrm{D}}{\mathrm{d}t}\right|_{\mathrm{flow,CCR,relax}} + r_\mathrm{det}\frac{f}{1-f}\left(\boldsymbol{Q}_\mathrm{A} - \boldsymbol{Q}_\mathrm{D}\right). \tag{10}$$

At equilibrium with no flow, Eq. (8) gives $f = \phi_\mathrm{as}$. All three equations include contributions from the rate of sticker attachment r_att, and a stretch-dependent rate of sticker detachment r_det, as defined in Eqs. (2) and (4). The latter terms in Eqs. (9) and (10) ensure that the stress remains constant upon attachment/detachment. This feature is due to the fact that, in the PETS model, $\boldsymbol{Q}_\mathrm{A}$ and $\boldsymbol{Q}_\mathrm{D}$ contain the nonlinear spring force.

The "flow,CCR,relax" term in Eq. (10) contains relaxation mechanisms similar to the "classic" RP model, Eq. (5). However, because attached chains are "clamped" on both ends, the "flow,CCR" term of Eq. (9) only contains CCR relaxation, as in Eq. (3). See Table I for the full equation set.

Important parameters of the PETS model are (i) parameters reminiscent of the "classic" RP model [44]: the orientation, τ_d, and stretch, τ_s, relaxation times of the (unattached) chain; (ii) sticker parameters: τ_as and ϕ_as; (iii) finite extensibility parameter: the maximum stretch ratio λ_max of the chain (as the maximum stretch is approached, the polymeric stress, the rate of stretch relaxation, and the rate of sticker dissociation all diverge). Typically, for real systems such as "sticky" entangled telechelic stars, as reported in Ref. [52], $(1-\phi_\mathrm{as}) \ll 1$ and $\tau_\mathrm{s} \ll \tau_\mathrm{d} \ll \tau_\mathrm{as}$. For the majority of this work, we therefore choose $\tau_\mathrm{s} = 1$, $\tau_\mathrm{d} = 10^2$, $\tau_\mathrm{as} = 10^3$, to represent experiments. Also, we choose $\lambda_\mathrm{max} = 10$ (unless otherwise stated). In the PETS model, increasing λ_max has a clear influence on the predictions in nonlinear shear or extensional flows, at flow rates greater than the inverse effective stretch time, τ_s^{-1}, or

inverse of the association time, τ_{as}^{-1}, whichever is smaller. In shear flow, at high flow rates, increasing λ_{max} increases the strain value at which the stress is maximum and also increases the steady state stress value; however, the maximum stress value is nearly unchanged. In extensional flow, at high extension rates, increasing λ_{max} increases the maximum stress value, the steady state stress value, and the strain at which the maximum stress occurs. The influence of λ_{max} can be seen, e.g., by looking at Fig. 11, where $\lambda_{max} = 40$.

It is worth noting that the "two state" nature of the PETS model shares some similarities with other constitutive models for supramolecular systems. As discussed in the Introduction, there are several models available for telechelic linear polymers forming flowerlike micelles in the unentangled state, e.g. Ref. [40, 41]. Another similar model is the the VCM model [53] often used for wormlike micellar solutions, which can be thought of as arising from the joining together of linear chains with sticky groups at either end to form longer linear chains. The critical difference as compared to the PETS model is that, for a wormlike micelle in the "attached" state, reptation is still possible and can relax stress: the VCM model reflects this. In contrast, in the PETS model, stress relaxation is suppressed in the attached state. For this reason, the PETS model most likely should not be applied to wormlike micelles without further modification. It is also worth mentioning that in other "two-state" models such as the VCM model [53] or Ref. [40, 41] for unentangled telechelic chains, stress is *not* conserved upon attachment and detachment of chains, whilst (as noted above) the PETS model does ensure that stress is conserved.

III. SHEAR BANDING SIMULATIONS

A. Flow curve and shear banding

We briefly summarize the phenomenology of shear banding. Fig. 3 presents a sketch of the steady state shear stress as a function of the applied shear rate, typically for $\boldsymbol{\sigma}$ following the Rolie-Poly model [54] with $\beta \approx 0$, i.e. no CCR [55]. Other models that exhibit shear banding, e.g. the Johnson-Segalman [45] model, often have a similar steady state stress curve [25]. The (non-monotonic) homogeneous constitutive curve is "ABCDEF". The system is unstable in the portion "CD", and often considered to be metastable in the "BC" and "DE" portions (though global stability analysis remains an open question [25, 56]). The (shear banded)

TABLE I. Preaveraged model (PETS) equation set [39].

Expression for the stress tensor, in units of G:

$$\boldsymbol{\sigma} = f\boldsymbol{Q}_\mathrm{A} + (1-f)\boldsymbol{Q}_\mathrm{D}.$$

Evolution of the fraction of attached chains:

$$\frac{\mathrm{d}f}{\mathrm{d}t} = r_\mathrm{att}\,(1-f) - r_\mathrm{det}f.$$

Evolution of the attached chains tensor:

$$\frac{\mathrm{d}\boldsymbol{Q}_\mathrm{A}}{\mathrm{d}t} = \boldsymbol{g}\,(\boldsymbol{Q}_\mathrm{A}) + \frac{1}{3\lambda_\mathrm{max}^2 - 3}\,\mathrm{tr}\,[\boldsymbol{g}\,(\boldsymbol{Q}_\mathrm{A})]\,\boldsymbol{Q}_\mathrm{A} + r_\mathrm{att}\frac{1-f}{f}\,(\boldsymbol{Q}_\mathrm{D} - \boldsymbol{Q}_\mathrm{A})\,,$$

with

$$\boldsymbol{g}\,(\boldsymbol{Q}_\mathrm{A}) \equiv \boldsymbol{\kappa}\cdot\boldsymbol{Q}_\mathrm{A} + \boldsymbol{Q}_\mathrm{A}\cdot\boldsymbol{\kappa}^\mathrm{T} - 2\beta\tilde{\nu}\lambda_\mathrm{A}^{-1}\,(\boldsymbol{Q}_\mathrm{A} - \mathrm{f}_\mathrm{E}(\lambda_\mathrm{A})\boldsymbol{I})\,.$$

Evolution of the detached chains tensor:

$$\frac{\mathrm{d}\boldsymbol{Q}_\mathrm{D}}{\mathrm{d}t} = \boldsymbol{h}\,(\boldsymbol{Q}_\mathrm{D}) + \frac{1}{3\lambda_\mathrm{max}^2 - 3}\,\mathrm{tr}\,[\boldsymbol{h}\,(\boldsymbol{Q}_\mathrm{D})]\,\boldsymbol{Q}_\mathrm{D} + r_\mathrm{det}\frac{f}{1-f}\,(\boldsymbol{Q}_\mathrm{A} - \boldsymbol{Q}_\mathrm{D})\,,$$

with

$$\boldsymbol{h}\,(\boldsymbol{Q}_\mathrm{D}) \equiv \boldsymbol{\kappa}\cdot\boldsymbol{Q}_\mathrm{D} + \boldsymbol{Q}_\mathrm{D}\cdot\boldsymbol{\kappa}^\mathrm{T} - 2\beta\tilde{\nu}\lambda_\mathrm{D}^{-1}\,(\boldsymbol{Q}_\mathrm{D} - \mathrm{f}_\mathrm{E}(\lambda_\mathrm{D})\boldsymbol{I}) - \frac{1}{\tau_\mathrm{d}}\,(\boldsymbol{Q}_\mathrm{D} - \mathrm{f}_\mathrm{E}(\lambda_\mathrm{D})\boldsymbol{I}) - \frac{2(1-\lambda_\mathrm{D}^{-1})}{\tau_\mathrm{s}}\,\mathrm{f}_\mathrm{E}(\lambda_\mathrm{D})\boldsymbol{Q}_\mathrm{D}.$$

Preaveraged CCR rate:

$$\tilde{\nu} = (1-f)\frac{1-\lambda_\mathrm{D,eq}^{-1}}{\tau_\mathrm{s}}\,\mathrm{f}_\mathrm{E}(\lambda_\mathrm{D,eq}) + f\,r_\mathrm{det}\frac{\lambda_\mathrm{A} - \lambda_\mathrm{D}}{(\lambda_\mathrm{A} + \lambda_\mathrm{D})}.$$

Evolution of the CCR stretch-variable:

$$\frac{\mathrm{d}\lambda_\mathrm{D,eq}}{\mathrm{d}t} = (\boldsymbol{\kappa} : \boldsymbol{Q}_\mathrm{D}/\,\mathrm{tr}\,\boldsymbol{Q}_\mathrm{D})\lambda_\mathrm{D,eq} - \frac{\lambda_\mathrm{D,eq} - 1}{\tau_\mathrm{s}}\,\mathrm{f}_\mathrm{E}(\lambda_\mathrm{D,eq}) + f\,r_\mathrm{det}(\lambda_\mathrm{A} - \lambda_\mathrm{D,eq}).$$

Rate of attachment and detachment:

$$r_\mathrm{att} = \tau_\mathrm{as}^{-1}\frac{\phi_\mathrm{as}}{1-\phi_\mathrm{as}}, \quad r_\mathrm{det}(\lambda_\mathrm{A}) = \tau_\mathrm{as}^{-1}\left(\frac{1 - \lambda_\mathrm{A}^2\lambda_\mathrm{max}^{-2}}{1 - \lambda_\mathrm{max}^{-2}\left(\lambda_\mathrm{A} - \frac{r}{Za_0}\right)^2}\right)^{-\frac{3}{2}Z\lambda_\mathrm{max}^2}.$$

Stretch of the attached and detached chains:

$$\lambda_\mathrm{A} = \left(\frac{\lambda_\mathrm{max}^2\,\mathrm{tr}\,(\boldsymbol{Q}_\mathrm{A})}{3\lambda_\mathrm{max}^2 - 3 + \mathrm{tr}\,(\boldsymbol{Q}_\mathrm{A})}\right)^{1/2}, \quad \lambda_\mathrm{D} = \left(\frac{\lambda_\mathrm{max}^2\,\mathrm{tr}\,(\boldsymbol{Q}_\mathrm{D})}{3\lambda_\mathrm{max}^2 - 3 + \mathrm{tr}\,(\boldsymbol{Q}_\mathrm{D})}\right)^{1/2}.$$

Finite extensibility function:

$$\mathrm{f}_\mathrm{E}(\lambda) = \frac{1 - \lambda_\mathrm{max}^{-2}}{1 - \lambda^2\lambda_\mathrm{max}^{-2}}.$$
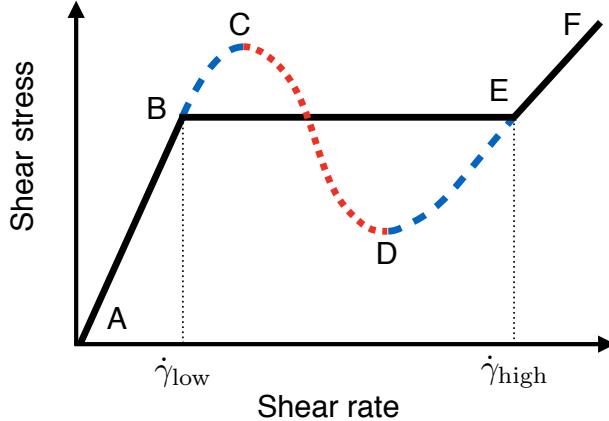
FIG. 3. Steady state shear stress function of the applied shear rate. The "ABCDEF" line is the (non-monotonic) homogeneous constitutive curve, while the "ABEF" path is the shear-banded flow curve. The selected stress is the "BE" level and the selected shear rates are $\dot{\gamma}_{\text{low}}$ and $\dot{\gamma}_{\text{high}}$.

flow curve is "ABEF", i.e. when the applied shear rate, $\dot{\gamma}_{\text{av}}$, is between $\dot{\gamma}_{\text{low}}$ and $\dot{\gamma}_{\text{high}}$, the system spontaneously forms two macroscopic bands of fluid, one at a shear rate $\dot{\gamma}_{\text{low}}$ and the other at $\dot{\gamma}_{\text{high}}$ [29]. In the banded regime, i.e. $\dot{\gamma}_{\text{low}} < \dot{\gamma}_{\text{av}} < \dot{\gamma}_{\text{high}}$, the stress stays constant, or slightly increases due to curvature effects (not considered here) in geometries such as cylindrical Couette [57–59].

For an applied shear rate such that $\dot{\gamma}_{\text{low}} < \dot{\gamma}_{\text{av}} < \dot{\gamma}_{\text{high}}$, the fraction, α_{high}, of fluid "experiencing" the high shear rate is given by the lever rule:

$$\dot{\gamma}_{\text{av}} \approx \alpha_{\text{high}}\dot{\gamma}_{\text{high}} + (1 - \alpha_{\text{high}})\dot{\gamma}_{\text{low}}. \tag{11}$$

This rule has been confirmed by many experiments [26]. The stress selection that is made by the system when it bands, which corresponds to the stress plateau "BE" in Fig. 3, is unique if we include a diffusion term in our model [60].

In what follows, we present the geometry, the method used to derive the diffusion terms (that allow a single stress selection) as well as the simulation set-up, followed by our results and discussion.

B. Parallel plates

We consider a parallel plate configuration: the top plate at $y = L$ moves with velocity u in the x-direction with respect to the bottom plate at $y = 0$, giving fixed average shear rate
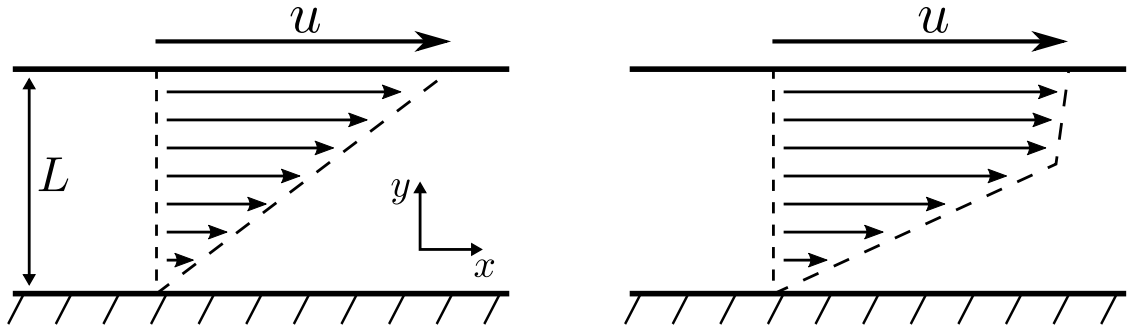
FIG. 4. Simulation set-up. The top plate at $y = L$ moves with a velocity u in the x-direction with respect to the bottom plate at $y = 0$. Left: homogeneous flow. Right: a banded flow.

$\dot{\gamma}_{\mathrm{av}} = u/L$, cf. Fig. 4. This may describe a cone-plate or Taylor-Couette flow, if we neglect the curvature effects.

C. Diffusive terms

In order to study the shear banding effects associated with the set of equations presented in Table I, we detail (in Appendix A) the effect of diffusion of the chains across a unidimensional channel. We split the domain between $y = 0$ and $y = L$ into a set of "boxes" of size Δy, and we consider the effect of chains "jumping" between these boxes. We suppose that there are n chains in total in each box, a fraction f of which are attached and a fraction $(1 - f)$ detached. We then assume that at each time step Δt, each box exchanges δn chains with each of the adjacent boxes. These chains are selected in proportion to the number of attached or detached chains in the box from which they leave.

The derivation of the diffusive terms is done in Appendix A, and the resulting equations, which act in addition to the dynamics listed in Table I, are:

$$\frac{\partial f}{\partial t} = D \frac{\partial^2 f}{\partial y^2}, \tag{12}$$

$$\frac{\partial f \boldsymbol{Q}_{\mathrm{A}}}{\partial t} = D \frac{\partial^2 f \boldsymbol{Q}_{\mathrm{A}}}{\partial y^2}, \tag{13}$$

$$\frac{\partial (1 - f) \boldsymbol{Q}_{\mathrm{D}}}{\partial t} = D \frac{\partial^2 (1 - f) \boldsymbol{Q}_{\mathrm{D}}}{\partial y^2}, \tag{14}$$

where D is the diffusion coefficient. The derivation of these equations, as presented in the Appendix, is based on a "toy" model for diffusion in which it is imagined that star arms (both attached and detached) hop back and forth, carrying their stress with them,

resulting in the symmetric set of equations above with a single diffusion constant. These equations are physical in the sense of being derived from a microscopic molecular model, albeit a highly idealized one. It is possible to imagine processes whereby both detached and attached arms could diffuse in a real physical system, even when noting that in practice both are connected to the branch point of the star. For example, when a detached arm relaxes, it gains freedom to move a short distance into a new region of space. When it does so, the rest of the entanglement matrix (comprising both attached and unattached arms) must correspondingly move in the opposite direction so as to maintain the overall incompressibility of the system. Relaxation of the detached arm also allows the star branch point to take a small "hop" in space, and permits surrounding chains to relax and move by constraint release. Through a succession of such processes, the entangled matrix, detached and attached arms, and branch points can all be carried diffusively back and forth. A more rigorous derivation should account for all these processes, and may result in effects whereby the detached arms effectively diffuse faster than the attached arms, or where the diffusion constant increases as the proportion of detached arms increases. For the present manuscript, we do not attempt a detailed derivation of diffusive terms based on these, or other, microscopic processes, but instead use the symmetric toy diffusion equations above.

The above discussion does highlight that it may be possible to consider a situation in which only one species diffuses – most likely the detached species – whilst not altering the stress from the other species, or the fraction f of attached species as a function of position. We tested such a scenario in which diffusion was applied only to the $\boldsymbol{Q}_{\mathrm{D}}$ variable. We found that, although $\boldsymbol{Q}_{\mathrm{D}}$ varied smoothly across the shear band interface, all other variables such as f, $\boldsymbol{Q}_{\mathrm{A}}$ and shear rate became discontinuous at the interface in our numerical scheme, i.e. the numerical solution was not smooth. As a result, the stress selection mechanism (which is one reason for including diffusion) appeared to be ineffective. Although we have not investigated this extensively, we do not presently believe that diffusion in only one of the species is sufficient to stabilize the bands.

D. Simulation method and parameters

The diffusion coefficient, D, is dimensionless in the simulations, as are the gap size L and timescales (e.g. τ_{as}, the longest relaxation time), corresponding to physical (dimensional)

quantities $\tilde{D}$, $\tilde{L}$ and $\tilde{\tau}_{\mathrm{as}}$ respectively. The dimensionless D may therefore be obtained from $D = \tilde{D}L^2\tilde{\tau}_{\mathrm{as}}/\tilde{L}^2\tau_{\mathrm{as}}$, so a decrease in physical gap size $\tilde{L}$ increases the dimensionless D. For the rest of this work, the (dimensionless) gap size is set as $L = 1$, without loss of generality.

Experimental methods can provide values of $\tilde{D}$ for: (i) linear entangled polymers, which range from 10^{-15} to 10^{-10} m^2/s [61–64], (ii) linear polymers with stickers along the backbone ranging from 10^{-12} to 10^{-15} m^2/s [65], or (iii) unentangled telechelic stars ranging from 10^{-14} to 10^{-13} m^2/s [66, 67].

To our knowledge, diffusion coefficients for entangled telechelic star polymers are not available in the literature but must somewhat fall within the ranges given above. Taking $\tilde{D} \sim 10^{-14}$ m^2/s, $\tilde{L} \sim 1$ mm, $\tilde{\tau}_{\mathrm{as}} \sim 10^6$ s, and $\tau_{\mathrm{as}} = 10^3$ (as used in Section IV to represent the experiments of Ref. [52]), gives a reference dimensionless diffusion coefficient $D_0 = 10^{-5}$. In the following, we vary D around D_0, noting that (for example) changes in gap height will substantially affect the dimensionless diffusion constant.

We use the fourth order Runge-Kutta (RK4) method to increment Eqs. (8) to (10), and the widely used [59, 68–70] Crank-Nicolson (CN) finite difference method [71] to increment the diffusive terms, Eqs. (12) to (14). To increment in time Eqs. (8) to (10), we could use a simple Euler scheme. We choose to use RK4 method which offers a good balance between order of accuracy and cost of computation. The CN method is a second order method in time and unconditionally stable. At each numerical time step, f, $\boldsymbol{Q}_{\mathrm{A}}$, and $\boldsymbol{Q}_{\mathrm{D}}$ are changed by Eqs. (8) to (10) using a RK4 step (flow contribution) and then via Eqs. (12) to (14) using a CN step (diffusion contribution).

We use a uniform spatial grid of $N_{\mathrm{grid}} \geq 1\,000$ points with a zero-gradient (Neumann) boundary condition imposed on the top and bottom plates, i.e. no quantity can exit the system:

$$\left.\frac{\partial X}{\partial y}\right|_{y=0} = 0 \quad \text{and} \quad \left.\frac{\partial X}{\partial y}\right|_{y=L} = 0, \tag{15}$$

where X is each of $\boldsymbol{Q}_{\mathrm{A}}$, $\boldsymbol{Q}_{\mathrm{D}}$, and f. Note that other boundary conditions could have been considered [72] but we use Eq. (15) since these are consistent with the assumed microscopic basis for the diffusion terms in our equations.

We use a (common) time step for the RK4 and CN methods that is smaller than the characteristic times of the system (τ_{as}, τ_{free}, $\dot{\gamma}^{-1}$) and smaller than the characteristic diffusion time across a box $\Delta t_{\mathrm{diff}} = (\Delta y)^2/D$, where $\Delta y = L/N_{\mathrm{grid}}$ is the box (grid) size. Therefore, a

finer grid (increase of N_{grid}) not only implies more computation points but could also imply a smaller simulation time step, (as Δy decreases), which would highly increase the simulation time. Nevertheless, we must ensure that the transition between the high and low share rate bands (if any) is "numerically smooth", see inserts of Fig. 8. The width of that interface, ℓ_{int}, is determined by the diffusion coefficient and a relaxation time as $\ell_{\mathrm{int}} \approx (D\tau)^{1/2}$ [73], and we must ensure that $\Delta y \ll \ell_{\mathrm{int}}$, so we take $\tau \equiv \tau_{\mathrm{s}}$ (the smallest relaxation time). Hence, a high number of grid points are needed for small-D simulations. In Section IV, we explore the effects of three values for the (dimensionless) diffusion coefficient: $D = \{10^{-7},\ 10^{-5},\ 10^{-3}\}$, with respectively $N_{\mathrm{grid}} = \{10\,000,\ 4\,000,\ 1\,000\}$, ensuring that $\Delta y \ll \ell_{\mathrm{int}}$. We have checked for convergence with respect to the size of the time-steps and space-steps.

E. Momentum equation in parallel plate geometry

The typical Reynolds number, R_{e}, is given by the balance between the inertia and viscosity as $R_{\mathrm{e}} = \rho u L/\mu$, where $\rho \approx 1$ g/cm^3 is the density of the polymer, $u \approx 1$ mm/s is the typical velocity, $L \approx 1$ mm is the typical gap size, and μ the polymer viscosity that we take of order 10^5 Pa·s [74]. Hence, $R_{\mathrm{e}} \approx 10^{-8} \ll 1$, so we can neglect the inertia contribution.

The momentum equation reads

$$\rho \mathrm{D}_t \boldsymbol{u} = \boldsymbol{\nabla} \cdot \boldsymbol{T}, \tag{16}$$

where $\mathrm{D}_t \equiv \partial_t + \boldsymbol{u} \cdot \boldsymbol{\nabla}$, and $\boldsymbol{T} = \boldsymbol{\sigma} + \eta(\boldsymbol{\kappa} + \boldsymbol{\kappa}^T) - p\boldsymbol{I}$ is the total stress with $\boldsymbol{\kappa} = (\boldsymbol{\nabla u})^T$ the velocity gradient tensor, $\boldsymbol{\sigma}$ the polymeric stress, η the Newtonian-solvent viscosity set as $\eta = 0.1$ for the rest of this work, and p the isotropic pressure ensuring incompressibility. Note that the viscosity is not a crucial parameter here as long as the Newtonian stress remains smaller than the polymeric stress, i.e. $\eta\dot{\gamma}_{\mathrm{av}} < \sigma_{xy}$.

A direct consequence of a small Reynolds number is that Eq. (16) becomes

$$\boldsymbol{\nabla} \cdot \boldsymbol{T} = \boldsymbol{0}. \tag{17}$$

Thus, $\partial T_{xy}/\partial y = 0$, so T_{xy} is constant across the gap. It follows that $T_{xy}(y,t) = \langle T_{xy}(y,t) \rangle$, where $\langle \, \cdot \, \rangle = \frac{1}{L} \int_0^L \cdot \, \mathrm{d}y$ is an average across the gap, with

$$T_{xy}(x,t) = \sigma_{xy}(y,t) + \eta\dot{\gamma}(y,t) \tag{18}$$

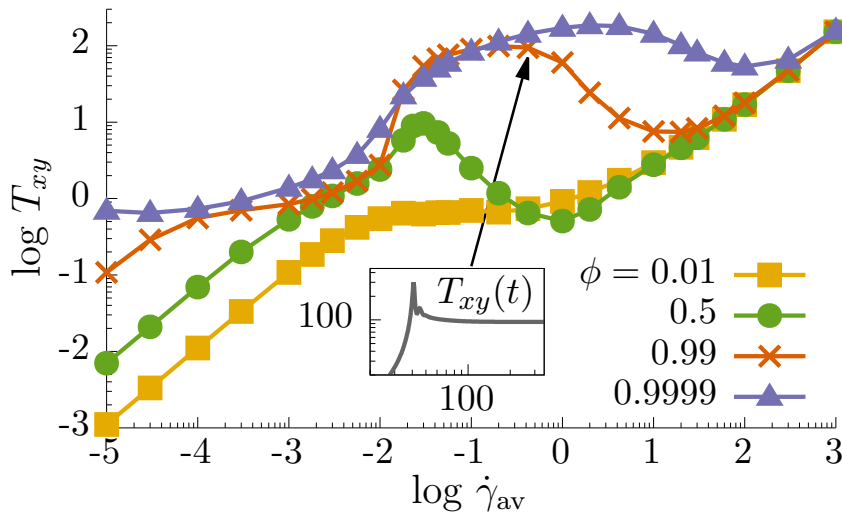$$\langle T_{xy}(y,t) \rangle = \langle \sigma_{xy}(y,t) \rangle + \eta \langle \dot{\gamma}(y,t) \rangle. \tag{19}$$

15

FIG. 5. Homogeneous flow curves of the PETS model [39] with $\phi_{as} = \{0.01, 0.5, 0.99, 0.9999\}$. In insert is $T_{xy}(t)$ for $\dot{\gamma}_{av} = 0.42$ and $\phi_{as} = 0.99$. Parameters are $\tau_s = 1$, $\tau_d = 10^2$, $\tau_{as} = 10^3$.

Combining the two above equations gives

$$\dot{\gamma}(y,t) = \langle \dot{\gamma}(y,t) \rangle + \frac{1}{\eta}\Big(\langle \sigma_{xy}(y,t) \rangle - \sigma_{xy}(y,t) \Big), \tag{20}$$

where $\langle \dot{\gamma}(y,t) \rangle \equiv \dot{\gamma}_{av}$ is the constant (externally) applied shear rate, or average shear rate across the gap, during step rate experiments or simulations.

At each time step, we compute the local value of the polymeric stress $\sigma_{xy}(y,t)$ using the set of equations Table I and Eqs. (12) to (14). Then, the average stress across the gap, $\langle \sigma_{xy}(y,t) \rangle$, is computed which, in turn, allows us to evaluate the local shear rate via Eq. (20). This local shear rate is then used in the next step to update the polymeric stress. We increment the dynamical equations for the system by repeating this cycle for each time step.

IV.   PREDICTIONS OF THE "DIFFUSIVE" PREAVERAGED MODEL

A.   PETS model: Homogeneous flow curves

In Fig. 5, we present the homogeneous (i.e. we force the system to remain homogeneous) constitutive flow curves of the PETS model where we vary the equilibrium fractions, ϕ_{as}, of attached stickers, i.e. we change the "stickiness" of the system from $\phi_{as} = 0.01$ (not

16

sticky) to $\phi_{as} = 0.9999$ (sticky). It is clear that, as ϕ_{as} increases, a non-monotonicity in the constitutive curve appears, and so shear banding phenomena may be anticipated. Additionally, as illustrated by the insert in Fig. 5, the transient stress during start-up of steady homogeneous flow exhibits a sharp stress maximum, which is a result of attached chains being stretched close to their maximum λ_{max} before the stickers are forced to detach. This detachment event, and subsequent relaxation of the detached chains, produces a rapid reduction of stress. We may anticipate that this produces interesting dynamical phenomena during the establishment of shear bands. We refer the reader to Section IV of Ref. [39] for a detailed explanation of the transient flow behavior depending on the parameter value. Note that, in the notation of Ref. [39], the flow curves represented here in Fig. 5 sit in regions C_1 for $\phi_{as} = 0.01$, intersection C_1/C_2 for $\phi_{as} = 0.5$, C_2 for $\phi_{as} = 0.99$, and A_1 for $\phi_{as} = 0.9999$.

The multiple transition that can be seen in Fig. 5 can be explained as follows. A first transition is seen at a flow rate, when $\dot{\gamma}_{av} \approx (\tau_d/1 - \phi_{as})^{-1}$. Then, there are three phenomena to consider:

(i) When $\dot{\gamma}_{av} > \tau_{as}^{-1} = 10^{-3}$, the attached chains (if any) start to stretch giving rise to an increase in T_{xy};

(ii) When $\dot{\gamma}_{av} > \tau_{free}^{-1}$, the fraction of attached arms (if any), f, drops. In effect, this decreases T_{xy} because when attached chains detach they can then relax their stretch. Note that, given Eq. (1), $\phi_{as} = \{0.01, \ 0.5, \ 0.99, \ 0.9999\}$ correspond to $\tau_{free}^{-1} = \{10^{-5}, \ 10^{-3}, \ 0.1, \ 10\}$ which are roughly the rates at which the stress decreases for each curve;

(iii) When $\dot{\gamma}_{av} > \tau_s^{-1} = 1$, detached chains start to stretch, giving rise to an increase in T_{xy}.

B. Banded flow curves

In the following, we explore the complex flow dynamics arising from the "PETS + diffusion" model, i.e. Table I and Eqs. (12) to (14), for $\phi_{as} = 0.99$ (sticky system) by means of 1-dimensional parallel plate simulations, as described Section III B.

At $t = 0$, the stress tensors $\boldsymbol{Q}_A$ and $\boldsymbol{Q}_D$ are set equal to the isotropic tensor, and the fraction of attached chains, f, is set as the fraction of attached chains at equilibrium, ϕ_{as},
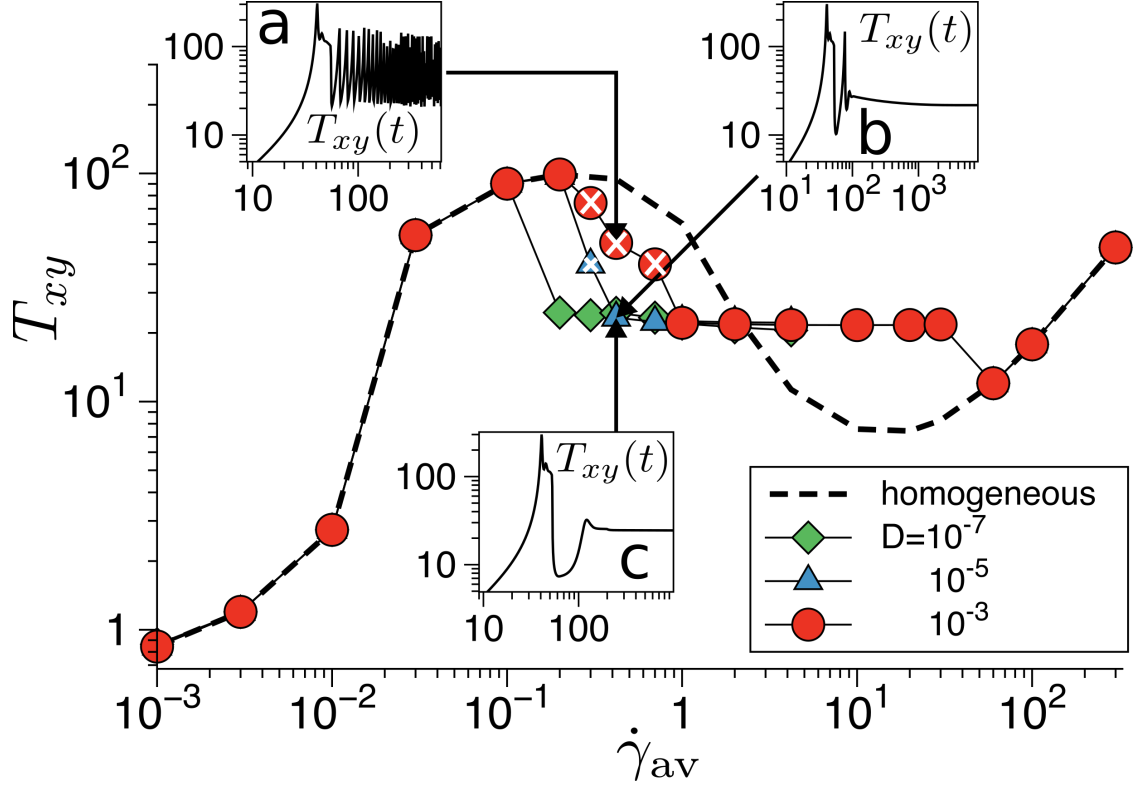
17

FIG. 6. Steady state stress versus shear rate for (forced) homogeneous flow (dashed line), and for shear banding simulations (symbols), time averaged in the case of oscillatory response (white crossed symbols). Inserts (a, b, c) show the transient stress versus time, $T_{xy}(t)$, at $\dot{\gamma}_{\mathrm{av}} = 0.42$, for $D = 10^{-3}$, $D = 10^{-5}$, and $D = 10^{-7}$ respectively. Parameters are $\tau_{\mathrm{s}} = 1$, $\tau_{\mathrm{d}} = 10^2$, $\tau_{\mathrm{as}} = 10^3$, $\phi_{\mathrm{as}} = 0.99$, $\lambda_{\max} = 10$.

plus a small perturbation,

$$f(y, t = 0) = \phi_{\mathrm{as}} + \xi \cos(\pi y), \tag{21}$$

where $\xi \ll \phi_{\mathrm{as}}$ is the overall amplitude of the perturbation, which ensures f to be slightly lower than ϕ_{as} at high y and vice versa. A small value of ξ leads to delayed effects, i.e. longer simulation time needed to access a banded state, while large values of ξ are unphysical – in the following, we use $\xi = 10^{-3}$. If banding occurs, Eq. (21) guarantees a high shear rate band at high y values, because f drops when the flow rate increases. Other initial conditions may result in bands (either oscillatory or steady) forming away from the wall, which typically migrate towards one wall or the other, see Section V.

In Fig. 6 we plot the steady state stress as a function of applied $\dot{\gamma}_{\mathrm{av}}$, for various diffusion coefficients around D_0, as discussed in Section III D. We also show transient plots of stress

18

versus time for different diffusion coefficient at the same $\dot{\gamma}_{\mathrm{av}} = 0.42$. We found that for large values of the diffusion coefficient and in a narrow range of applied shear rate, e.g. $D = 10^{-3}$ (equivalently, for small gap size) and $0.2 < \dot{\gamma}_{\mathrm{av}} < 1$, the total stress does not reach steady state but keeps oscillating (white crossed symbols) between, roughly, the stress values for homogeneous flow (dashed line) and for the shear banded state. Each "oscillation" appears to be, in detail, a sharp stress overshoot similar to the early event where initially attached chains reach their maximal stretch and detach. However, at smaller values of D, e.g. $D = 10^{-5}$ (equivalently, as the gap size increases), the stress oscillates for a short time, but a steady state is eventually reached. After a further decrease of D, e.g. $D = 10^{-7}$, no oscillation is seen.

Note that we also performed a simulation with $D = 10^{-3}$ (and all parameters identical to those in Fig. 6), where we imposed $\dot{\gamma}_{\mathrm{av}} = 30$, giving steady state shear banding. Once the steady banded state is reached, we decreased $\dot{\gamma}_{\mathrm{av}}$ rapidly (in a time scale of order τ_{free}) to $\dot{\gamma}_{\mathrm{av}} = 0.42$, i.e. a value where oscillations are expected. We saw that the oscillations showed up again, this time starting from a steady banded state, and the system reached the limit cycle that we found in Fig. 7 top right, described below.

C.   Stick-slip and diffusion

In order to investigate the transient behavior and especially the interesting oscillatory response further, we present, in Fig. 7, color maps (corresponding to the three inserts in Fig. 6) of $\dot{\gamma}(y, t)$ and $f(y, t)$, and the trajectory of the simulation projected onto the plane $(T_{xy}, \Delta f)$, where Δf is the difference between the maximum and minimum value of f observed across the gap.

Focusing first on $D = 10^{-7}$ in Fig. 7 left, we observe that the fraction of attached arms drops across the whole width of the simulation at the time ($t \approx 40$) of the initial sharp stress maximum, and at this point no significant banding is observed. The flow remains homogeneous (H) for a time, but the $(T_{xy}, \Delta f)$ plane reveals the growth of an instability in which Δf increases. Eventually, at $t \approx 54$, a thin band of material near the upper wall reaches a state with almost all chains detached, which gives rise to a sharp recoil (R), i.e. where coexistence of negative and positive shear rates is seen, see Fig. 8. This permits a release of the elastic energy stored in the remaining bulk of the material, driving the sharp
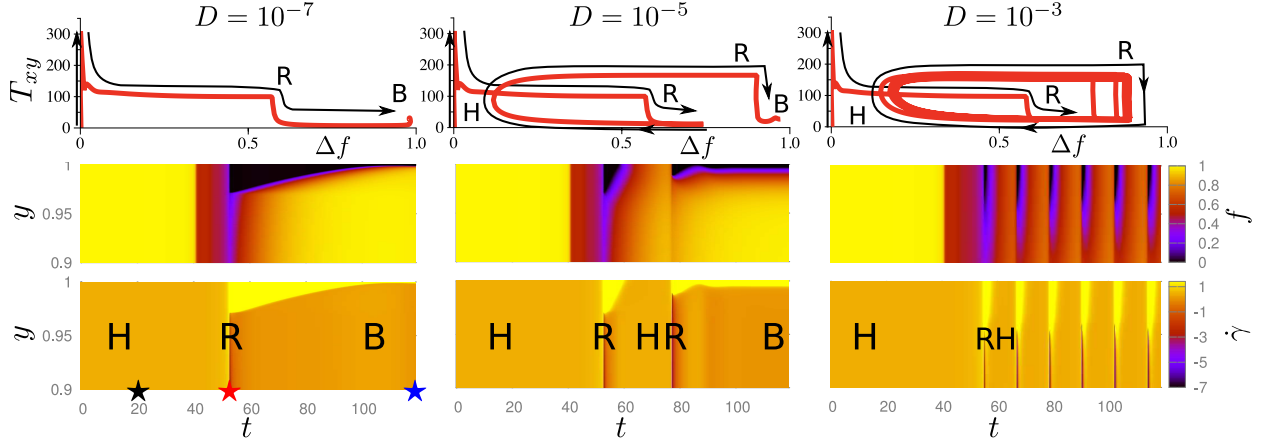
19

FIG. 7. Bottom to top: Time evolution of the spatially resolved local shear rate and fraction of attached chains, and of the stress versus Δf, for various diffusion coefficient and $\dot{\gamma}_{\mathrm{av}} = 0.42$. "H", "B", and "R" stand for homogeneous flow, (steady state) banded flow, and recoil, respectively. The highest values of $\dot{\gamma}$ have been truncated for clarity, and only $y > 0.9$ is shown. Parameters are $\phi_{\mathrm{as}} = 0.99$, $\xi = 10^{-3}$.

recoil and a rapid drop in stress. Subsequently, the flow stabilizes to a banded state (B), with a narrow band at high shear rate close to the upper wall, effectively an apparent wall slip. Fig. 8 displays the velocity profile during the homogeneous (H), recoil (R) and banded (B) states, at times indicated by stars in Fig. 7 left. We see in the $(T_{xy}, \Delta f)$ plane that the system is driven away from the instability and reaches a permanent banded state, where $\Delta f \approx 1$; two shear bands are formed, one with a high number of attached stickers, and the other with most of the stickers detached. In contrast, for larger $D = 10^{-5}$, shown in Fig. 7 middle, after the initial recoil the simulation returns towards a homogeneous state (H) before recoiling (R) once more and eventually stabilizing into a banded state (B) where, as before, $\Delta f \approx 1$. The $(T_{xy}, \Delta f)$ plane shows the extra oscillatory cycle made before the system eventually reaches a steady banded state.

For large values of the diffusion coefficient, e.g. $D = 10^{-3}$, oscillation between homogeneous (H) and recoil (R) states repeats indefinitely, i.e. no steady banded state is reached. The $(T_{xy}, \Delta f)$ plane, of Fig. 7 right, reveals the limit cycle that underpins the oscillations. Additionally, we provide snapshots of the simulation in Fig. 9, in which we can clearly identify the initial configuration ($t = 30$, top left), where the fraction of attached stickers seems homogeneous across the gap (due to $\xi \ll 1$ in Eq. (21)), and the velocity profile is a straight
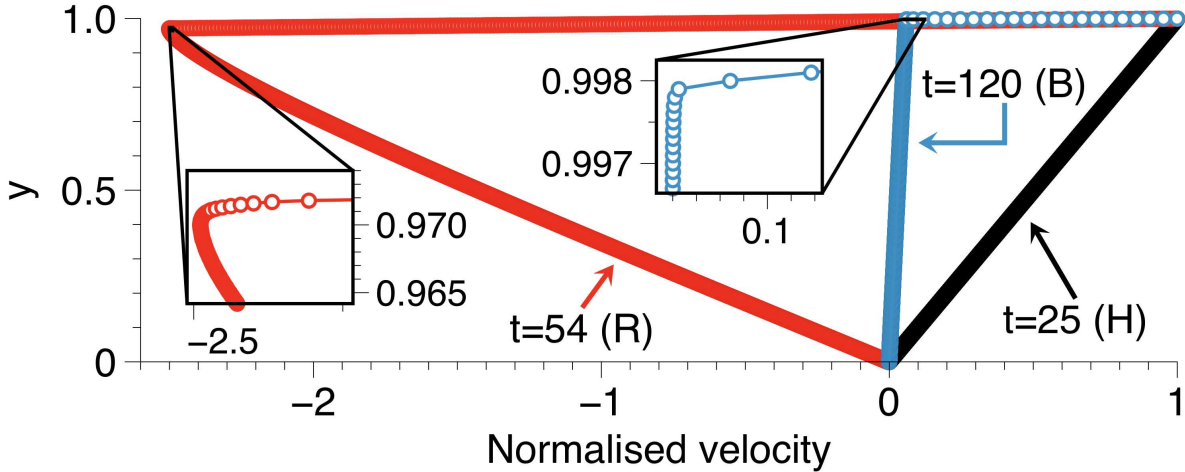
20

FIG. 8. Velocity profile (normalized by $\dot{\gamma}_{\mathrm{av}}$) for $D = 10^{-7}$ at times indicated by stars in Fig. 7.

line, indicating a homogeneous shear rate across the gap. Then, at $t = 55$ (Fig. 9 top right) we can see that the velocity profile is no longer linear and that the fraction of attached chains, f, has started to drop near $y = 1$. Subsequently, a snapshot at $t = 55.3$ (Fig. 9 bottom left) gives an indication of the severity of the recoil, which is driven by release of stored elastic energy in the material. A narrow band of material close to $y = 1$ has almost all its stickers detached ($f \approx 0$) and experiences high (positive) shear rates, while a large band with $f \approx 0.55$ has a relatively low and negative shear rate (i.e. it is recoiling). At this point it is worth emphasizing that the majority of the material has a *negative* velocity and only a thin band of material has a positive velocity. Experimentally, that would manifest in a large band of material going "backwards", i.e. in the direction opposite to the applied shear, while a narrow band of material would still flow in the direction of the applied shear. At a later time, $t = 65.4$ (Fig. 9 bottom right), the velocity profile is again nearly linear meaning that the shear rate is again nearly homogeneous across the gap, and that all the material is now flowing in the direction of the applied shear. Note that f has recovered to higher values (more stickers attached), which indicates that the material has self-healed: it nearly recovered all the bonds it had before the rupture [75].

Possible experimental verification of this phenomenon include velocimetry experiments where one could see the high shear rate band of material and a periodical recoil with some material going in the direction opposite to the applied shear.

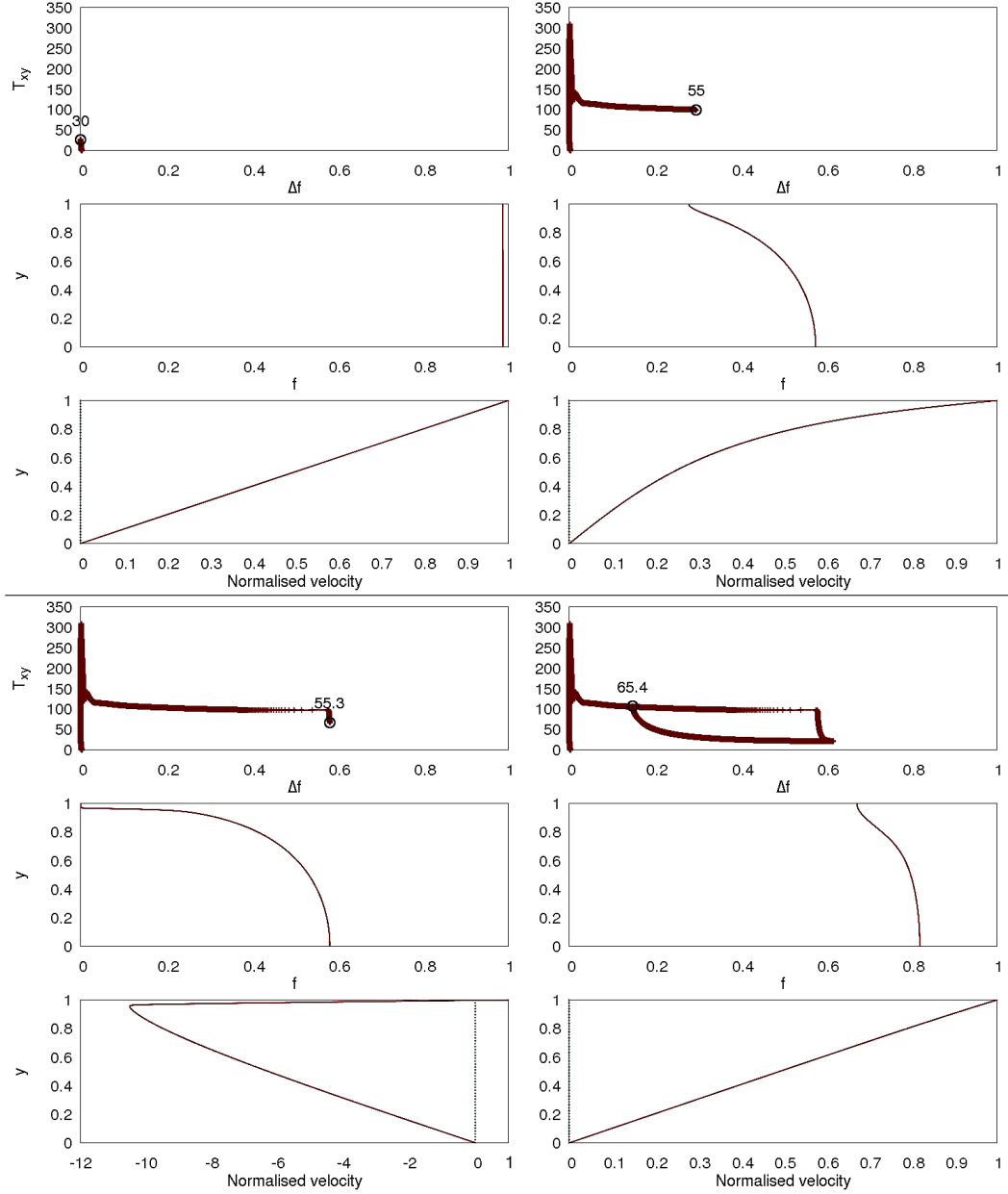The critical process driving the oscillation is the return towards a homogeneous flow

FIG. 9. Snapshots of the simulation at times $t = 30$, $t = 55$, $t = 55.3$, and $t = 65.4$ for $D = 10^{-3}$ in Fig. 7. We present the $(T_{xy}, \Delta f)$ plane, the fraction of associated stickers, f, across the gap, and the normalized (by $\dot{\gamma}_{\text{av}}$) velocity profile, form top to bottom respectively.

profile following the banding and elastic recoil. The dependence of this process on the diffusion constant indicates the following mechanism is at work: After the recoil, a narrow high shear rate band is formed, in which most chains are in the detached state. However, if diffusion is sufficiently rapid (depending upon the width of the band as well as the magnitude of the diffusion constant) diffusive exchange of chains between the narrow band and bulk of

the material (which contains many attached chains) leads to an increase in the number of attached chains in the "fast" band (seen as a reduction of Δf in the $(T_{xy}, \Delta f)$ trajectory). This slows down shear in the fast band, re-establishing a nearly homogeneous flow. This then sets up a state in which the initial banding and recoil instability can reoccur, so that the cycle potentially repeats indefinitely. The oscillation is therefore a result of interaction between the diffusion and the dynamics of the internal variables of the constitutive model.

Confirmation of this oscillatory mechanism is found by examining the effect of increasing shear rate. The oscillation is first seen for $\dot{\gamma}_{av}$ on the onset of the unstable region (negative slope of the constitutive curve, Fig. 5). The frequency of the oscillations increases almost linearly with increasing shear rate (circles Fig. 10), because the time needed for a chain to reach its maximum strain (followed by detachment and recoil) decreases as shear rate increases. Indeed, by analyzing the stress, T_{xy}, as a function of strain $\gamma = \dot{\gamma}_{av}t$, we see that the frequency of these oscillations is quasi-constant with increasing shear rate (squares Fig. 10). However, according to Eq. (11), the width of the high shear-rate band, $\alpha_{high}L$, also increases with increasing shear rate until, eventually, the band becomes sufficiently wide that diffusion can no longer re-establish a homogeneous flow profile. Beyond this point, oscillations are no longer seen.

Hence, there is a competition between two phenomena: (i) the homogenization of f across the gap via diffusion on a timescale $\tau_{dif} = (\alpha_{high}L)^2/D$, with $\alpha_{high} = (\dot{\gamma}_{av} - \dot{\gamma}_{low})/(\dot{\gamma}_{high} - \dot{\gamma}_{low})$ the fraction of gap occupied by the high shear rate band, from Eq. (11); and (ii) the breaking of the associated chains in the high shear rate band that occurs at a fixed strain γ_c, on a timescale $\tau_b = \gamma_c/\dot{\gamma}_{high}$. Thus, oscillations on the unstable branch of the flow are expected if $\tau_{dif} < \tau_b$, i.e. if $\dot{\gamma}_{av} < \dot{\gamma}_{av,c}$, where

$$\dot{\gamma}_{av,c} = \dot{\gamma}_{low} + (\dot{\gamma}_{high} - \dot{\gamma}_{low})(D\gamma_c/L^2\dot{\gamma}_{high})^{1/2} \tag{22}$$

is the critical shear rate above which no oscillations are expected. According to Fig. 6, $\dot{\gamma}_{high} \approx 130$, $\dot{\gamma}_{low} \approx 0.02$. Therefore, Eq. (22) gives $\dot{\gamma}_{av,c} = 1.5$ for $D = 10^{-3}$, and $\dot{\gamma}_{av,c} = 0.03$ for $D = 10^{-7}$ (which is before the unstable region), in qualitative agreement with Fig. 6. Note that the critical strain, γ_c, depends on the value of the maximum stretch ratio, λ_{max} as $\gamma_c \approx \sqrt{3}\lambda_{max}$.

We examine Eq. (22) further by investigating a broader range of parameters. In Figs. 11 and 12, we present the flow curves for various D, with $(\lambda_{max}, \tau_{as}) = (40, 10^3)$

and $(\lambda_{\mathrm{max}}, \tau_{\mathrm{as}}) = (10, 2 \times 10^2)$ respectively, and we indicate where oscillations are seen in the simulations (shaded zone), and the prediction of Eq. (22) (vertical dashed line). In Fig. 13 we compare directly the upper critical shear rate for oscillations, $\dot{\gamma}_{\mathrm{av,c}}$, as predicted by Eq. (22), with the simulation observations for the upper critical average shear rate. Although, in our simulations, the transition between oscillations and steady banded state is not exactly predicted by Eq. (22), as seen in Fig. 13, it nevertheless follows the same trend, i.e. oscillations are seen for a larger $\dot{\gamma}_{\mathrm{av}}$ interval as D increases, and the increase in the critical average shear rate with increasing λ_{max} is captured. Note that large D values broaden the transition between the high and low shear rate regions, to the extent that, at the largest D values we simulate (in Figs. 11 and 12), the "transition" region begins to span the width of the simulation. The discrepancy observed for large D values in Fig. 13 can be attributed to the fact that the lever rule, Eq. (11), which considers a sharp transition between high and low shear rate bands, no longer accurately describes the banded flow with "smooth" transition. Moreover, the breaking time, τ_{b}, will be affected by the presence of a broad range of high shear rates, and the diffusion time, τ_{dif}, will be affected by the proximity of the far boundary, leading to the failure of the scaling argument.

Given that such complications exist in the simulations, we consider that Eq. (22), and the underlying physics it represents, captures the essential features of the transition from oscillatory to non-oscillatory flow.

V.   INFLUENCE OF THE INITIAL PERTURBATION

In Section IV, the initial perturbation on the fraction of attached chains, f, was set was using Eq. (21), ensuring that f was slightly higher than ϕ_{as} near the upper wall ($y = 1$) and slightly lower than ϕ_{as} near the lower wall ($y = 0$) which guaranteed that, when banding occurs, the high shear rate band is located near the upper wall.

A symmetric initial perturbation such as

$$f(y) = \phi_{\mathrm{as}} + \xi \cos(2\pi y) \tag{23}$$

ensures that, initially, the minimum of f is located at the center of the gap. Using Eq. (23) as initial condition, we observe that

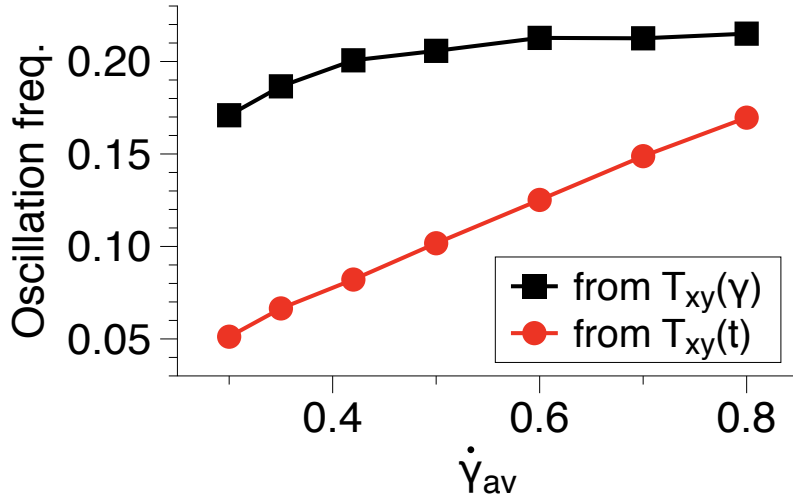(i) When steady banding occurs, the high shear rate band remains in the center of the

FIG. 10. Frequency of the oscillations as a function of the applied shear rate, corresponding to $D = 10^{-3}$ in Fig. 7. Red circles: for the stress vs time curve. Black squares: for the stress vs strain curve.
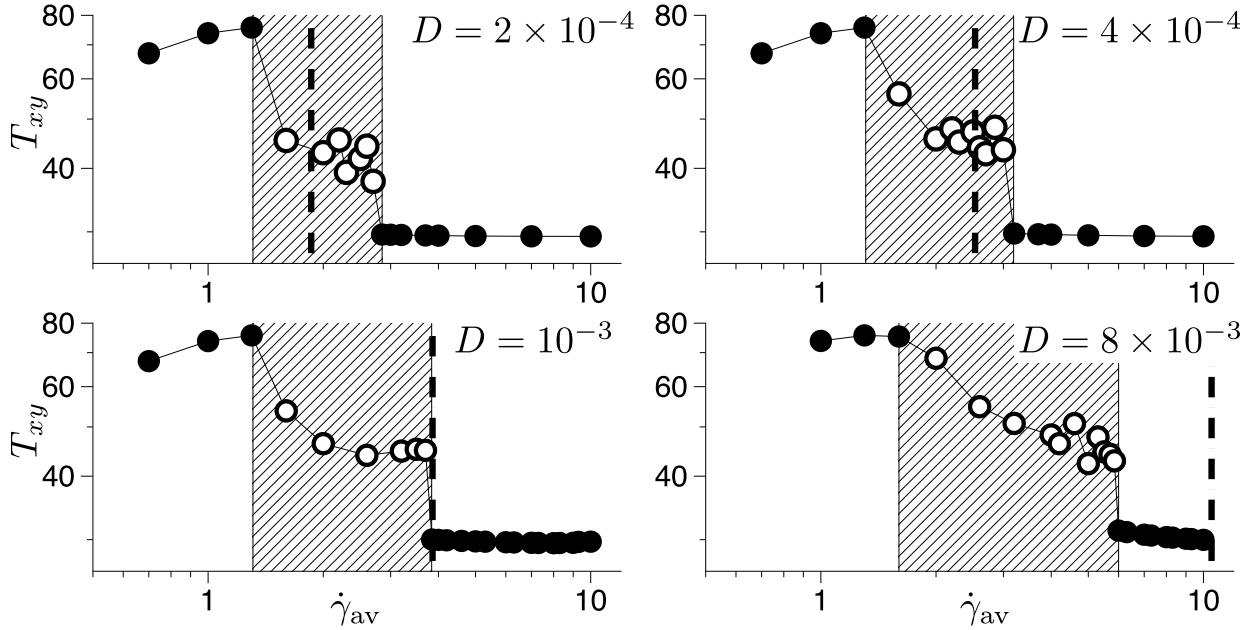

FIG. 11. Flow curves for $(\lambda_{\max}, \tau_{\mathrm{as}}) = (40, 10^3)$, and various D. The shaded zone and empty symbols indicate where oscillations are seen in the simulations, and the vertical dashed line is the prediction of Eq. (22).
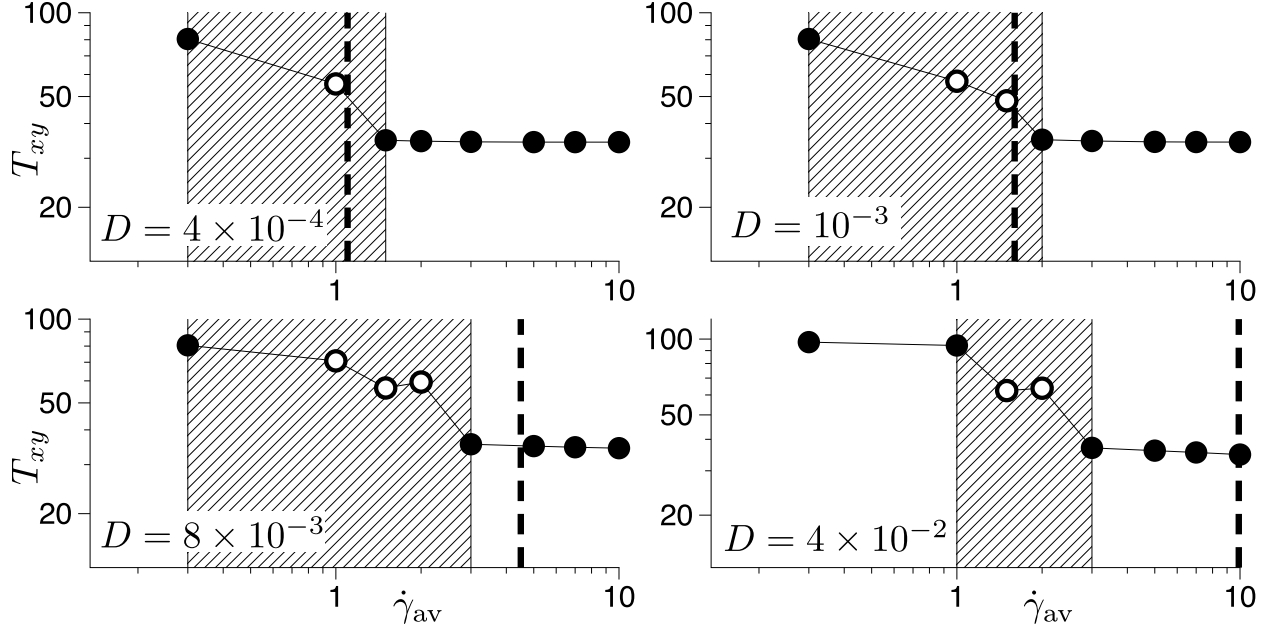
FIG. 12. Flow curves for $(\lambda_{\mathrm{max}}, \tau_{\mathrm{as}}) = (10, 2 \times 10^2)$, and various D. The shaded zone and empty symbols indicate where oscillations are seen in the simulations, and the vertical dashed line is the prediction of Eq. (22).
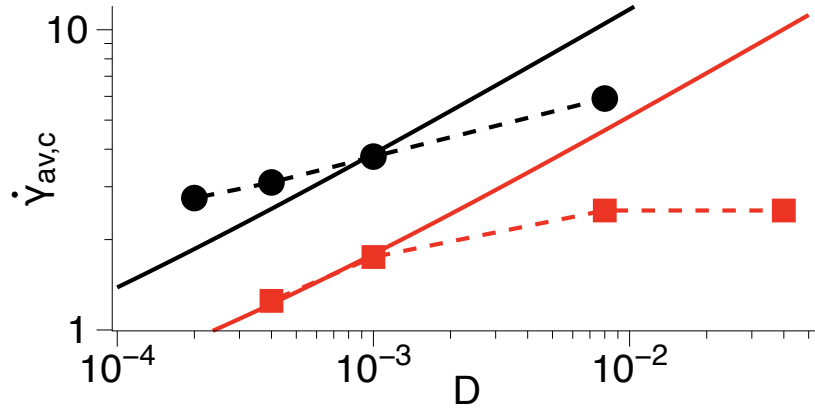

FIG. 13. Critical shear rate as a function of the diffusion coefficient from simulation (symbols) and from Eq. (22) (continuous lines) corresponding to Fig. 11 (top curves) and Fig. 12 (bottom curves).

gap;

(ii) When oscillations occur (in a range of shear rates), the high shear rate band appears in the center of the gap;

(iii) The range of shear rates at which ("permanent") oscillations are produced is slightly larger, e.g. for $D = 10^{-3}$, we see permanent oscillations for $\dot{\gamma}_{\mathrm{av}} = 1$, see Fig. 14 left, whereas at that shear rate the system stabilizes into a steady banded state when f is initialized using Eq. (21).

These results support the idea that diffusion destabilizes the bands, especially observation (iii), since when the high shear rate band is in the center of the simulation "box", diffusion from above and below the band rehomogenizes the flow. Hence the effect of the diffusion of the attached chains from the low shear rate band to the high shear rate band is stronger when the high shear rate band is in the center of the domain as compared to the edge, and we therefore expect oscillations when $\tau_{\mathrm{dif}}/2 < \tau_{\mathrm{b}}$.

The above situation, with the shear band, or stick-slip behavior, in the middle of the gap is in fact linear unstable to small perturbations and the band will eventually drift towards the upper or lower plate. We demonstrate this drift starting from an asymmetric initial condition. Focusing on $\dot{\gamma}_{\mathrm{av}} = 1$, we can set the initial perturbation such that f has its lowest value at $y = 1/3$,

$$
f(y) = \begin{cases} \phi_{\mathrm{as}} + \xi \cos(3\pi y), & 0 \le y \le 2/3 \\ \phi_{\mathrm{as}} + \xi, & 2/3 < y \le 1 \end{cases} \tag{24}
$$

the high shear rate band is initially formed at around $y = 1/3$, then it is slowly "pushed" to the bottom, cf. Fig. 14 right. When the high shear rate band reaches the bottom wall, oscillations cease for that particular shear rate ($\dot{\gamma}_{\mathrm{av}} = 1$), which is consistent with our initial results, Section IV.

Finally, if the initial perturbation is a random noise, then, when shear banding occurs, high shear rate front(s) appear across the gap at random places. When there are several high shear rate fronts, they eventually merge into one and is then "pushed" up or down at the wall, similarly to what is seen in Fig. 14 right.

VI. CONCLUSIONS

We have investigated shear instabilities using the novel constitutive law designed for describing the rheology of entangled telechelic star polymers of Ref. [39]. We augmented the
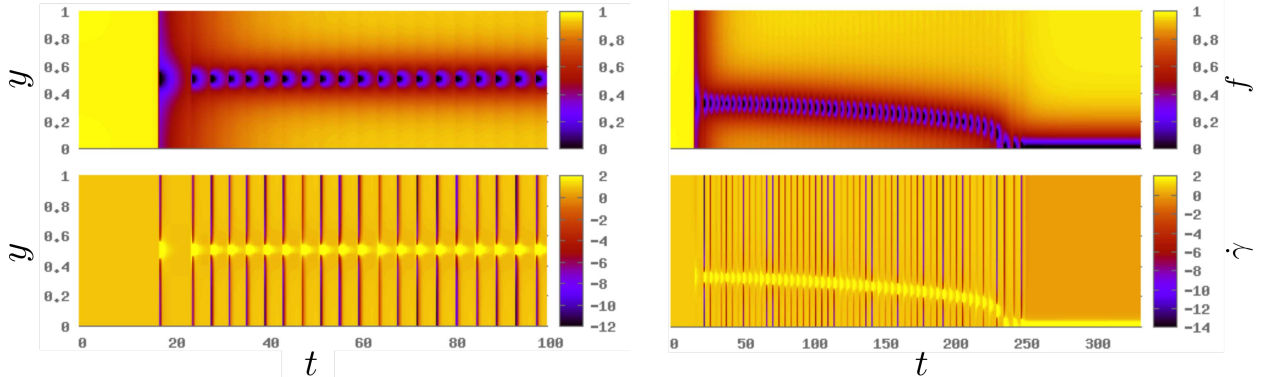
27

FIG. 14. Time evolution spatially resolved of f and $\dot{\gamma}$ for an initial perturbation set as Eq. (23) (left), and Eq. (24) (right).

model by including a diffusive term and performed simulations in a parallel plate configuration. The model displays shear banding, often accompanied by a strong elastic recoil in the transient response. This may appear as an "apparent" wall slip, i.e. a very narrow band of high shear rate close to the wall. In the same sense, the model also displays an oscillatory "apparent" stick-slip behavior, driven by a cycle of elastic recoil followed by diffusive rehomogenization of the flow. We link the oscillations unambiguously to the diffusion of the attached chains (with sticker attached) from the low shear rate band to the high shear rate band which destabilizes the banded structure. Interestingly, experimental data [36] shows a large noise (oscillations) on the stress response corresponding to the establishment of the banded structure, which is precisely where we found, in our model, the oscillations.

Since our modelling is entirely at the continuum level, with an imposed no-slip boundary condition, it is wholly impossible for these observed phenomena to be anything but "apparent" wall slip or stick-slip. Within this continuum approach, reducing the diffusion constant, or (correspondingly) increasing the gap size, removes the oscillations. Nevertheless, we may speculate that an identical mechanism drives stick-slip oscillations in the case of "true" wall slip, which occurs as a result of the microscopic local environment close to a wall, corresponding to a few polymer chain radii. Here, the physics governing chain conformations and dynamics can be quite different from the material bulk, and can include, for example, perturbation of the chain conformations by the hard wall, or physical bonding of chains to the wall. It seems very plausible that molecular diffusion from the material bulk into the local wall region might temporarily arrest wall slip (i.e. rehomogenizes the flow) before

28

wall slip occurs once more, driving a similar cyclic phenomenon to the one we observe. In the case of true wall slip, the local environment sets a new physical lengthscale (e.g. via the chain dimensions), so that increasing the (macroscopic) gap size no longer removes the oscillations.

Recent experiments on concentrated solution of telechelic polymers showed the following results: (i) stress maxima at a constant strain, (ii) shear banding [33], (iii) oscillatory/chaotic transient stress response [36, 37]. With supporting evidence, these effects were attributed to "a mechanical instability at the interface between coexisting bands" rather than to stick-slip at the walls. An underlying transport process was suggested [36], though the existence of this was identified from the long time to reach steady state, rather than as a factor in the oscillatory or chaotic response. Some, but not all, of the studied materials were in the concentrated regime where chains become entangled [36]. The observed stress maxima, shear banding and oscillatory response are in qualitative agreement with our findings. Our results indicate that the presence of a transport process could be a contributing factor in transient response, in addition to determining stress selection at steady state. Nevertheless, there remain differences, e.g. we have not observed a chaotic response. We may speculate that these differences could be due to differences in the precise constitutive behavior, or to the three dimensional character of the flow which is beyond the presently reported simulations (e.g. they could be observing an elastic flow instability leading to the chaotic response, which would not be captured in our 1D model).

The mechanism of rehomogenization of the fraction of attached stickers can be seen as a self-healing mechanism through chain reassociation into a network structure. To design surfaces with adjusted friction properties, an important objective in a large number of practical situations, it is crucial to understand the mechanisms at work. For example, some experiments have evidenced a stick-slip phenomenon in non-sticky entangled systems [76], gels [77–79], or lubricants [80]. The work presented in this article could have a potential impact on these other area and give some insights to understand the complex phenomenon leading to stick-slip.

Appendix A: Derivation of the diffusive terms

Theories for polymer migration, such as the two-fluid model, usually involve incorporating into the mass balance equation a polymer stress-diffusion term, which can be derived in a variety of ways [81, 82]. Other approach, such as "body tensor continuum theory" proposed by Öttinger [83] result in mass transport terms that include the divergence of the stress tensor. More recently, Larson and co-workers [84, 85] developed a continuum theory that demonstrated how the divergence of stress arises as a result of defining local polymer mass by the local density of beads rather than by the density of molecular centers of mass, leading to a coupling of polymer stress relaxation to center-of-mass migration.

In this work, we derive the diffusive terms based on a molecular picture that at each time step Δt, there is a small quantity δn of material leaving the box y towards the $(y + \Delta y)$ box (and a same quantity δn arrives from that box), and a quantity δn of material leaving the box y towards the $(y - \Delta y)$ box (and a same quantity δn arrives from that box), see Fig. 15. Therefore, our system is set so that it is incompressible.

At each time step, the box at "height" y loses stress related to the attached and detached population in proportion to

$$2\delta n f(y)\boldsymbol{Q}_{\mathrm{A}}(y), \tag{A1}$$

$$2\delta n\big(1 - f(y)\big)\boldsymbol{Q}_{\mathrm{D}}(y), \tag{A2}$$

where the factor 2 comes from the fact that, except at the boundaries, the quantities exit through the top *and* bottom. Moreover, at each time step, the box at "height" y gains some stress coming from the top and bottom boxes:

from A-chains

$$\delta n(f\boldsymbol{Q}_{\mathrm{A}})(y + \Delta y) + \delta n(f\boldsymbol{Q}_{\mathrm{A}})(y - \Delta y), \tag{A3}$$

from D-chains

$$\delta n\big((1 - f)\boldsymbol{Q}_{\mathrm{D}}\big)(y + \Delta y) + \delta n\big((1 - f)\boldsymbol{Q}_{\mathrm{D}}\big)(y - \Delta y), \tag{A4}$$

where we used the shorthand $(f\boldsymbol{Q})(y) \equiv f(y)\boldsymbol{Q}(y)$, and all the quantities are at time t.

Now, we can express the fraction of attached chains, f, at $t + \Delta t$. Considering that the total number of chains in the box at "height" y is n, the number of attached chains at time $t + \Delta t$ is

$$
\begin{aligned}
nf(y, t + \Delta t) &= (n - 2\delta n)f(y) + \delta n f(y + \Delta y) + \delta n f(y - \Delta y) \\
&= nf(y) + \delta n\big(f(y + \Delta y) + f(y - \Delta y) - 2f(y)\big),
\end{aligned} \tag{A5}
$$

where all quantities are evaluated at time t if not specified otherwise. Dividing by $n\Delta t$ and rearranging the terms, we recognize the finite difference approximation of the time derivative and second order spatial derivative derivative, so that in the limit $\Delta t \to 0$ and $\Delta y \to 0$, taken such that $(\Delta y)^2/\Delta t$ remains constant, we find:

$$
\frac{\partial f}{\partial t} = D\frac{\partial^2 f}{\partial y^2}, \tag{A6}
$$

where $D = \dfrac{\delta n}{n}\dfrac{(\Delta y)^2}{\Delta t}$. Hence, the fraction of attached chains, f, diffuses across the boxes with a diffusion coefficient D.

Now, we will derive the value of the tensor $\boldsymbol{Q}_{\mathrm{A}}$ at time $t + \Delta t$. According to the balance equations previously written we have that the total stress in the box at "height" y from the
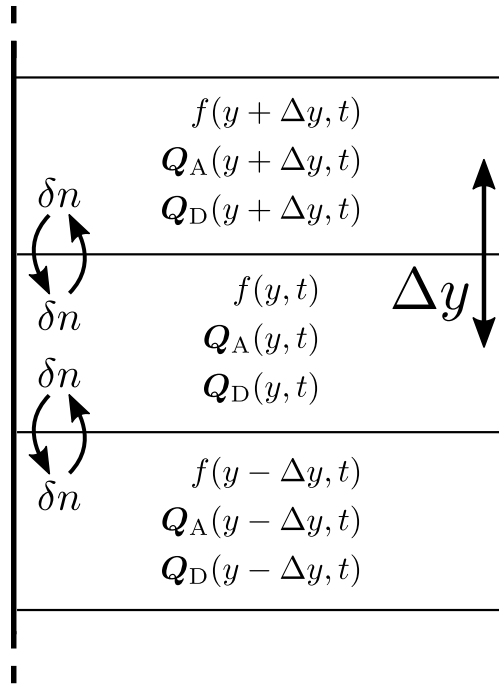

FIG. 15. Diffusion across the simulation boxes.

31

attached population is

$$
\begin{aligned}
n f(y, t + \Delta t) \boldsymbol{Q}_\mathrm{A}(y, t + \Delta t) ={} & \text{(stress from A-chains at time } t \text{ in box } y) \\
& - \text{(stress from A-chains leaving box } y) \\
& + \text{(stress from A-chains arriving box } y) \\
={} & n(f\boldsymbol{Q}_\mathrm{A})(y, t) \\
& - 2\delta n(f\boldsymbol{Q}_\mathrm{A})(y, t) \\
& + \delta n\big((f\boldsymbol{Q}_\mathrm{A})(y + \Delta y, t) + (f\boldsymbol{Q}_\mathrm{A})(y - \Delta y, t) \big).
\end{aligned}
$$

Rearranging the terms and approximating the finite differences for the derivatives, we obtain the partial differential equation

$$
\frac{\partial f\boldsymbol{Q}_\mathrm{A}}{\partial t} = D\frac{\partial^2 f\boldsymbol{Q}_\mathrm{A}}{\partial y^2}. \tag{A7}
$$

From Eq. (12), we know the value of $f(y, t + \Delta t)$, hence we can deduce the value of $\boldsymbol{Q}_\mathrm{A}(y, t + \Delta t)$ from Eq. (13) by a simple division.

Similarly, the time evolution of the tensor $\boldsymbol{Q}_\mathrm{D}$ representing the detached chains can be obtained via

$$
\frac{\partial (1 - f)\boldsymbol{Q}_\mathrm{D}}{\partial t} = D\frac{\partial^2 (1 - f)\boldsymbol{Q}_\mathrm{D}}{\partial y^2}. \tag{A8}
$$

---

[1] Larson, R. G., "Instabilities in viscoelastic flows," *Rheol. Acta* **31**, 213–263 (1992).

[2] Bird, R. B., R. C. Armstrong, and O. Hassager, "Fluid mechanics," *Dyn. Polym. Liq.*, (Wiley Inteterscience, New York, 1987), vol. 1.

[3] Maxwell, B., and J. C. Galt, "Velocity profiles for polyethylene melt in tubes," *J. Polym. Sci.* **62**, S50–S53 (1962).

[4] Vinogradov, G. V., V. P. Protasov, and V. E. Dreval, "The rheological behavior of flexible-chain polymers in the region of high shear rates and stresses, the critical process of spurting, and supercritical conditions of their movement at T>Tg," *Rheol. Acta* **23**, 46–61 (1984).

[5] Brochard, F., and P.-G. de Gennes, "Shear-dependent slippage at a polymer/solid interface," *Langmuir* **8**, 3033–3037 (1992).

[6] Migler, K. B., H. Hervet, and L. Leger, "Slip transition of a polymer melt under shear stress," *Phys. Rev. Lett.* **70**, 287–290 (1993).

[7] Brochard-Wyart, F., C. Gay, and P.-G. de Gennes, "Slippage of Polymer Melts on Grafted Surfaces," *Macromolecules* **29**, 377–382 (1996).

[8] Benbow, J. J., and P. Lamb, "New aspects of melt fracture," *Polym. Eng. Sci.* **3**, 7–17 (1963).

[9] Paskhin, E. D., "Motion of polymer liquids under unstable conditions and in channel terminals," *Rheol. Acta* **17**, 663–675 (1978).

[10] Leonov, A. I., "A linear model of the stick-slip phenomena in polymer flow in rheometers," *Rheol. Acta* **23**, 591–600 (1984).

[11] den Otter, J. L., "Some investigations of melt fracture," *Rheol. Acta* **10**, 200–207 (1971).

[12] Lupton, J. M., and H. W. Regester, "Melt flow of polyethylene at high rates," *Polym. Eng. Sci.* **5**, 235–245 (1965).

[13] Soltero, J. F. A., F. Bautista, J. E. Puig, and O. Manero, "Rheology of Cetyltrimethylammonium p -ToluenesulfonateWater System. 3. Nonlinear Viscoelasticity," *Langmuir* **15**, 1604–1612 (1999).

[14] Bandyopadhyay, R., G. Basappa, and A. K. Sood, "Observation of Chaotic Dynamics in Dilute Sheared Aqueous Solutions of CTAT," *Phys. Rev. Lett.* **84**, 2022–2025 (2000).

[15] Denn, M. M., "Extrusion Instabilities and Wall Slip," *Annu. Rev. Fluid Mech.* **33**, 265–287 (2001).

[16] Goddard, J. D., "Material Instability In Complex Fluids," *Annu. Rev. Fluid Mech.* **35**, 113–133 (2003).

[17] Koopmans, R., J. Den Doelder, and J. Molenaar, *Polymer melt fracture*, (CRC Press, 2010).

[18] Divoux, T., M. A. Fardin, S. Manneville, and S. Lerouge, "Shear Banding of Complex Fluids," *Annu. Rev. Fluid Mech.* **48**, 150724171740009 (2015).

[19] Cates, M. E., "Nonlinear viscoelasticity of wormlike micelles (and other reversibly breakable polymers)," *J. Phys. Chem.* **94**, 371–375 (1990).

[20] Cates, M. E., "Reptation of Living Polymers: Dynamics of Entangled Polymers in the Presence of Reversible Chain-Scission Reactions," *Macromolecules* **20**, 2289–2296 (1987).

[21] Spenley, N. A., M. E. Cates, and T. C. B. McLeish, "Nonlinear rheology of wormlike micelles," *Phys. Rev. Lett.* **71**, 939–942 (1993).

[22] Spenley, N. A., X. F. Yuan, and M. E. Cates, "Nonmonotonic Constitutive Laws and the Formation of Shear-Banded Flows," *J. Phys. II* **6**, 551–571 (1996).

[23] Cates, M. E., and S. M. Fielding, "Rheology of giant micelles," *Adv. Phys.* **55**, 799–879 (2006).

[24] Fielding, S. M., "Complex dynamics of shear banded flows," *Soft Matter* **3**, 1262–1279 (2007).

[25] Olmsted, P. D., "Perspectives on shear banding in complex fluids," *Rheol. Acta* **47**, 283–300 (2008).

[26] Lerouge, S., and J. F. Berret, "Shear-induced transitions and instabilities in surfactant worm-like micelles," *Adv. Polym. Sci.* **230**, 1–71 (2010).

[27] Dealy, J. M., and R. G. Larson, *Structure and Rheology of Molten Polymers*, (Carl Hanser Verlag GmbH & Co. KG, München, 2006), 2 edn.

[28] McLeish, T. C. B., and R. C. Ball, "A molecular approach to the spurt effect in polymer melt flow," *J. Polym. Sci. Part B Polym. Phys.* **24**, 1735–1745 (1986).

[29] Fielding, S. M., "Triggers and signatures of shear banding in steady and time-dependent flows," *J. Rheol.* **60**, 821–834 (2016).

[30] Moorcroft, R. L., and S. M. Fielding, "Shear banding in time-dependent flows of polymers and wormlike micelles," *J. Rheol.* **58**, 103 (2014).

[31] Manneville, S., "Recent experimental probes of shear banding," *Rheol. Acta* **47**, 301–318 (2008).

[32] Cao, J., and A. E. Likhtman, "Shear banding in molecular dynamics of polymer melts," *Phys. Rev. Lett.* **108**, 1–5 (2012).

[33] Berret, J.-F., and Y. Séréro, "Evidence of Shear-Induced Fluid Fracture in Telechelic Polymer Networks," *Phys. Rev. Lett.* **87**, 048303 (2001).

[34] Ligoure, C., and S. Mora, "Fractures in complex fluids: The case of transient networks," *Rheol. Acta* **52**, 91–114 (2013).

[35] Sprakel, J., E. Spruijt, J. van der Gucht, J. T. Padding, and W. J. Briels, "Failure-mode transition in transient polymer networks with particle-based simulations," *Soft Matter* **5**, 4748 (2009).

[36] Sprakel, J., E. Spruijt, M. A. Cohen Stuart, N. A. M. Besseling, M. P. Lettinga, and J. van der Gucht, "Shear banding and rheochaos in associative polymer networks," *Soft Matter* **4**, 1696–1705 (2008).

[37] Michel, E., J. Appell, F. Molino, J. Kieffer, and G. Porte, "Unstable flow and nonmonotonic flow curves of transient networks," *J. Rheol.* **45**, 1465–1477 (2001).

[38] Castillo-Tejas, J., S. Carro, and O. Manero, "Shear Banding in Telechelic Associative Polymers by Molecular Dynamics," *ACS Macro Lett.* **6**, 190–193 (2017).

[39] Boudara, V. A. H., and D. J. Read, "Stochastic and preaveraged nonlinear rheology models for entangled telechelic star polymers," *J. Rheol.* **61**, 339–362 (2017).

[40] Tripathi, A., K. C. Tam, and G. H. McKinley, "Rheology and Dynamics of Associative Polymers in Shear and Extension: Theory and Experiments," *Macromolecules* **39**, 1981–1999 (2006).

[41] Vaccaro, A., and G. Marrucci, "A model for the nonlinear rheology of associating polymers," *J. Nonnewton. Fluid Mech.* **92**, 261–273 (2000).

[42] Picard, G., A. Ajdari, L. Bocquet, and F. Lequeux, "Simple model for heterogeneous flows of yield stress fluids," *Phys. Rev. E* **66**, 051501 (2002).

[43] Head, D. A., A. Ajdari, and M. E. Cates, "Rheological instability in a simple shear-thickening model," *Europhys. Lett.* **57**, 120–126 (2002).

[44] Likhtman, A. E., and R. S. Graham, "Simple constitutive equation for linear polymer melts derived from molecular theory: Rolie-Poly equation," *J. Nonnewton. Fluid Mech.* **114**, 1–12 (2003).

[45] Johnson, M., and D. Segalman, "A model for viscoelastic fluid behavior which allows non-affine deformation," *J. Nonnewton. Fluid Mech.* **2**, 255–270 (1977).

[46] Fardin, M. A., T. J. Ober, C. Gay, G. Grégoire, G. H. McKinley, and S. Lerouge, "Potential ways of thinking about the shear-banding phenomenon," *Soft Matter* **8**, 910–922 (2012).

[47] Marrucci, G., "Dynamics of entanglements: A nonlinear model consistent with the Cox-Merz rule," *J. Nonnewton. Fluid Mech.* **62**, 279–289 (1996).

[48] Brassinne, J., C.-A. Fustin, and J.-F. Gohy, "Polymer Gels Constructed Through Metal-Ligand Coordination," *J. Inorg. Organomet. Polym. Mater.* **23**, 24–40 (2013).

[49] Nair, K. P., V. Breedveld, and M. Weck, "Multiresponsive Reversible Polymer Networks Based on Hydrogen Bonding and Metal Coordination," *Macromolecules* **44**, 3346–3357 (2011).

[50] Weng, W., J. B. Beck, A. M. Jamieson, and S. J. Rowan, "Understanding the mechanism of gelation and stimuli-responsive nature of a class of metallo-supramolecular gels," *J. Am. Chem. Soc.* **128**, 11663–11672 (2006).

[51] Kramers, H., "Brownian motion in a field of force and the diffusion model of chemical reactions," *Physica* **7**, 284–304 (1940).

[52] van Ruymbeke, E., D. Vlassopoulos, M. Mierzwa, T. Pakula, D. Charalabidis, M. Pitsikalis, and N. Hadjichristidis, "Rheology and Structure of Entangled Telechelic Linear and Star

Polyisoprene Melts," *Macromolecules* **43**, 4401–4411 (2010).

[53] Vasquez, P. A., G. H. McKinley, and L. Pamela Cook, "A network scission model for wormlike micellar solutions. I. Model formulation and viscometric flow predictions," *J. Nonnewton. Fluid Mech.* **144**, 122–139 (2007).

[54] Graham, R. S., A. E. Likhtman, T. C. B. McLeish, and S. T. Milner, "Microscopic theory of linear, entangled polymer chains under rapid deformation including chain stretch and convective constraint release," *J. Rheol.* **47**, 1171–1200 (2003).

[55] Agimelen, O. S., and P. D. Olmsted, "Apparent Fracture in Polymeric Fluids Under Step Shear," *Phys. Rev. Lett.* **110**, 204503 (2013).

[56] Sato, K., X. F. Yuan, and T. Kawakatsu, "Why does shear banding behave like first-order phase transitions? Derivation of a potential from a mechanical constitutive model," *Eur. Phys. J. E* **31**, 135–144 (2010).

[57] Lerouge, S., J. P. Decruppe, and J. F. Berret, "Correlations between rheological and optical properties of a micellar solution under shear banding flow," *Langmuir* **16**, 6464–6474 (2000).

[58] Fielding, S. M., and P. D. Olmsted, "Flow phase diagrams for concentration-coupled shear banding," *Eur. Phys. J. E* **11**, 65–83 (2003).

[59] Olmsted, P. D., O. Radulescu, and C.-Y. D. Lu, "JohnsonSegalman model with a diffusion term in cylindrical Couette flow," *J. Rheol.* **44**, 257–275 (2000).

[60] Lu, C. Y. D., P. D. Olmsted, and R. C. Ball, "Effects of Non-local Stress on the Determination of Shear Banding Flow," *Phys. Rev. Lett.* **84**, 642–645 (2000).

[61] Lodge, T. P., "Reconciliation of the Molecular Weight Dependence of Diffusion and Viscosity in Entangled Polymers," *Phys. Rev. Lett.* **83**, 3218–3221 (1999).

[62] Tao, H., T. P. Lodge, and E. D. von Meerwall, "Diffusivity and Viscosity of Concentrated Hydrogenated Polybutadiene Solutions," *Macromolecules* **33**, 1747–1758 (2000).

[63] Appel, M., and G. Fleischer, "Investigation of the chain length dependence of self-diffusion of poly(dimethylsiloxane) and poly(ethylene oxide) in the melt with pulsed field gradient NMR," *Macromolecules* **26**, 5520–5525 (1993).

[64] Wheeler, L. M., and T. P. Lodge, "Tracer diffusion of linear polystyrenes in dilute, semidilute, and concentrated poly(vinyl methyl ether) solutions," *Macromolecules* **22**, 3399–3408 (1989).

[65] Hackelbusch, S., T. Rossow, P. van Assenbergh, and S. Seiffert, "Chain Dynamics in Supramolecular Polymer Networks," *Macromolecules* **46**, 6273–6286 (2013).

[66] Rossow, T., A. Habicht, and S. Seiffert, "Relaxation and Dynamics in Transient Polymer Model Networks," *Macromolecules* **47**, 6473–6482 (2014).

[67] Tang, S., A. Habicht, S. Li, S. Seiffert, and B. D. Olsen, "Self-Diffusion of Associating Star-Shaped Polymers," *Macromolecules* **49**, 5599–5608 (2016).

[68] Adams, J. M., S. M. Fielding, and P. D. Olmsted, "Transient shear banding in entangled polymers: A study using the Rolie-Poly model," *J. Rheol.* **55**, 1007–1032 (2011).

[69] Fielding, S. M., and P. D. Olmsted, "Nonlinear dynamics of an interface between shear bands," *Phys. Rev. Lett.* **96**, 15–18 (2006).

[70] Germann, N., L. P. Cook, and A. N. Beris, "Investigation of the inhomogeneous shear flow of a wormlike micellar solution using a thermodynamically consistent model," *J. Nonnewton. Fluid Mech.* **207**, 21–31 (2014).

[71] Crank, J., and P. Nicolson, "A practical method for numerical evaluation of solutions of partial differential equations of the heat-conduction type," *Math. Proc. Cambridge Philos. Soc.* **43**, 50–67 (1947).

[72] Adams, J., S. Fielding, and P. Olmsted, "The interplay between boundary conditions and flow geometries in shear banding: Hysteresis, band configurations, and surface transitions," *J. Nonnewton. Fluid Mech.* **151**, 101–118 (2008).

[73] Fardin, M.-A., O. Radulescu, A. Morozov, O. Cardoso, J. Browaeys, and S. Lerouge, "Stress diffusion in shear banding wormlike micelles," *J. Rheol.* **59**, 1335–1362 (2015).

[74] Fetters, L. J., A. D. Kiss, D. S. Pearson, G. F. Quack, and F. J. Vitus, "Rheological behavior of star-shaped polymers," *Macromolecules* **26**, 647–654 (1993).

[75] Stukalin, E. B., L.-H. Cai, N. A. Kumar, L. Leibler, and M. Rubinstein, "Self-Healing of Unentangled Polymer Networks with Reversible Bonds," *Macromolecules* **46** (2013).

[76] Hervet, H., and L. Léger, "Flow with slip at the wall: from simple to complex fluids," *Comptes Rendus Phys.* **4**, 241–249 (2003).

[77] Baumberger, T., and C. Caroli, "Solid friction from stickslip down to pinning and aging," *Adv. Phys.* **55**, 279–348 (2006).

[78] Baumberger, T., C. Caroli, and O. Ronsin, "Self-healing slip pulses and the friction of gelatin gels," *Eur. Phys. J. E* **11**, 85–93 (2003).

[79] Kajiya, T., A. Daerr, T. Narita, L. Royon, F. Lequeux, and L. Limat, "Advancing liquid contact line on visco-elastic gel substrates: stick-slip vs. continuous motions," *Soft Matter* **9**,

454–461 (2013).

[80] Gourdon, D., and J. N. Israelachvili, "Transitions between smooth and complex stick-slip sliding of surfaces," *Phys. Rev. E* **68**, 021602 (2003).

[81] Mavrantzas, V. G., and A. N. Beris, "Modeling of the rheology and flow-induced concentration changes in polymer solutions," *Phys. Rev. Lett.* **69**, 273–276 (1992).

[82] Beris, A. N., and V. G. Mavrantzas, "On the compatibility between various macroscopic formalisms for the concentration and flow of dilute polymer solutions," *J. Rheol.* **38**, 1235–1250 (1994).

[83] Öttinger, H. C., "Incorporation of polymer diffusivity and migration into constitutive equations," *Rheol. Acta* **31**, 14–21 (1992).

[84] Zhu, G., H. Rezvantalab, E. Hajizadeh, X. Wang, and R. G. Larson, "Stress-gradient-induced polymer migration: Perturbation theory and comparisons to stochastic simulations," *J. Rheol.* **60**, 327–343 (2016).

[85] Hajizadeh, E., and R. G. Larson, "Stress-gradient-induced polymer migration in TaylorCouette flow," *Soft Matter* **13**, 5942–5949 (2017).